Check for updates

AGU ADVANCING EARTH AND SPACE SCIENCE

JGR Oceans

RESEARCH ARTICLE
10.1029/2021JC017608

Special Section:
Southern Ocean and Climate: Biogeochemical and Physical Fluxes and Processes

Key Points:

- Antarctic meltwater and projected wind stress change cause surface warming in the Weddell Sea and cooling in the rest of the Southern Ocean
- The subsurface response on the West Antarctic shelf differs between the models; one yields strong cooling and the other strong warming
- The mean-state representation and acceleration of the Antarctic Slope Current is the key process to explaining the differing shelf response

Correspondence to:
R. L. Beadling,
rebecca.beadling@noaa.gov

Citation:
Beadling, R. L., Krasting, J. P., Griffies, S. M., Hurlin, W. J., Bronselaer, B., Russell, J. L., et al. (2022). Importance of the Antarctic Slope Current in the Southern Ocean response to ice sheet melt and wind stress change. *Journal of Geophysical Research: Oceans*, *127*, e2021JC017608. https://doi.org/10.1029/2021JC017608

Received 25 MAY 2021
Accepted 8 APR 2022

Author Contributions:
Conceptualization: B. Bronselaer
Formal analysis: R. L. Beadling, G. A. MacGilchrist
Funding acquisition: J. L. Russell
Investigation: R. L. Beadling, J.-E. Tesdal
Methodology: R. L. Beadling, J. P. Krasting, S. M. Griffies, W. J. Hurlin, B. Bronselaer, M. Winton
Resources: J. P. Krasting, S. M. Griffies, W. J. Hurlin, M. Winton
Software: W. J. Hurlin
Supervision: J. P. Krasting, S. M. Griffies, M. Winton
Validation: R. L. Beadling, G. A. MacGilchrist

© 2022. American Geophysical Union. All Rights Reserved.

Importance of the Antarctic Slope Current in the Southern Ocean Response to Ice Sheet Melt and Wind Stress Change

R. L. Beadling[1,2,3], J. P. Krasting[2], S. M. Griffies[2,3], W. J. Hurlin[2], B. Bronselaer[2,3,4,5], J. L. Russell[5], G. A. MacGilchrist[2,3], J.-E. Tesdal[2,3], and M. Winton[2]

[1]University Corporation for Atmospheric Research, Boulder, CO, USA, [2]Geophysical Fluid Dynamics Laboratory, NOAA, Princeton, NJ, USA, [3]Princeton University Atmospheric and Oceanic Sciences Program, Princeton, NJ, USA, [4]British Petroleum, London, UK, [5]Department of Geosciences, University of Arizona, Tucson, AZ, USA

Abstract We use two coupled climate models, GFDL-CM4 and GFDL-ESM4, to investigate the physical response of the Southern Ocean to changes in surface wind stress, Antarctic meltwater, and the combined forcing of the two in a pre-industrial control simulation. The meltwater cools the ocean surface in all regions except the Weddell Sea, where the wind stress warms the near-surface layer. The limited sensitivity of the Weddell Sea surface layer to the meltwater is due to the spatial distribution of the meltwater fluxes, regional bathymetry, and large-scale circulation patterns. The meltwater forcing dominates the Antarctic shelf response and the models yield strikingly different responses along West Antarctica. The disagreement is attributable to the mean-state representation and meltwater-driven acceleration of the Antarctic Slope Current (ASC). In CM4, the meltwater is efficiently trapped on the shelf by a well resolved, strong, and accelerating ASC which isolates the West Antarctic shelf from warm offshore waters, leading to strong subsurface cooling. In ESM4, a weaker and diffuse ASC allows more meltwater to escape to the open ocean, the West Antarctic shelf does not become isolated, and instead strong subsurface warming occurs. The CM4 results suggest a possible negative feedback mechanism that acts to limit future melting, while the ESM4 results suggest a possible positive feedback mechanism that acts to accelerate melt. Our results demonstrate the strong influence the ASC has on governing changes along the shelf, highlighting the importance of coupling interactive ice sheet models to ocean models that can resolve these dynamical processes.

Plain Language Summary As the climate warms, the winds over the Southern Ocean (SO) are expected to increase in strength and shift southward and the Antarctic Ice Sheet (AIS) is expected to continue to melt. Both changes alter ocean circulation in the SO. We investigated the impact of these changes on the physical properties and circulation in the SO in a preindustrial control background state using two coupled climate models with different representations of the Antarctic Slope Current (ASC). In both models, we found an inhomogeneous surface response to these changes. The altered wind stress caused warming of the surface in the Weddell Sea, while the freshwater from the AIS caused surface cooling in the rest of the SO. On the West Antarctic shelf, where most of the observed ice-shelf melting occurs, the models produced very different responses. In one model, the meltwater elicits a strong subsurface cooling response which would act to limit further melt. In the other model, the meltwater causes a strong subsurface warming response which would act to accelerate further melt. The differing representations of the ASC explain this striking disagreement between the two models.

1. Introduction

The Southern Ocean (SO) plays a dominant role in the oceanic uptake of anthropogenic heat and carbon, accounting for over 40% of the oceanic carbon uptake (Frölicher et al., 2015) and 67%–98% of the global ocean heat gain (Frölicher et al., 2015; Roemmich et al., 2015), yet only having 33% of the World Ocean surface area. This role is a product of the unique and complex circulation in the SO that allows for the efficient exchange of properties between the atmosphere and the interior ocean. Two major changes are occurring and projected to strengthen throughout the 21st century which might alter SO circulation: an increase and poleward shift of the Southern Hemisphere westerlies (Goyal et al., 2021; Swart & Fyfe, 2012; D. W. J. Thompson et al., 2011) and an increase in meltwater from the Antarctic Ice Sheet (AIS; DeConto & Pollard, 2016; Rignot et al., 2013, 2019; The IMBIE team, 2018). These two processes exert competing effects on the stratification of the SO and the large-scale ocean circulation. Recent work utilizing model simulations and autonomous float and ship-based observations of the

21699291, 2022, 5, Downloaded from https://agupubs.onlinelibrary.wiley.com/doi/10.1029/2021JC017608 by University Of St Andrews University, Wiley Online Library on [08/11/2022]. See the Terms and Conditions (https://onlinelibrary.wiley.com/terms-and-conditions) on Wiley Online Library for rules of use; OA articles are governed by the applicable Creative Commons License

Visualization: R. L. Beadling
Writing – original draft: R. L. Beadling
Writing – review & editing: R. L. Beadling, J. P. Krasting, S. M. Griffies, G. A. MacGilchrist, J.-E. Tesdal, M. Winton

SO suggest that changes in wind and increased Antarctic meltwater may already be contributing to observed changes in temperature, salinity, and biogeochemical properties (Bronselaer et al., 2020).

Strengthened and poleward shifted Southern Hemisphere westerlies enhance ventilation of the ocean interior through increased upwelling of warm Circumpolar Deep Water (CDW) in the subpolar SO and increased formation of intermediate and mode waters at midlatitudes (Bronselaer et al., 2020; Russell et al., 2006; Spence et al., 2014; Waugh et al., 2019, 2021). Strengthened wind stress also influences large-scale circulation in the SO through the invigoration of baroclinic eddy activity which counteracts some of the enhancement to the overturning circulation driven by the strengthened surface Ekman transport (*eddy compensation;* Hallberg & Gnanadesikan, 2006; Morrison & Hogg, 2013). Wind-driven changes in the large-scale overturning circulation in the SO impact the uptake of anthropogenic heat and carbon (Bronselaer et al., 2020; Russell et al., 2006). Additionally, a poleward shift of the Southern Hemisphere jet impacts the strength of the coastal easterlies which exert a strong control on the properties of the waters on the Antarctic continental shelf. This has an influence on dense shelf water (DSW) production and the thermal properties of waters that directly interact with the Antarctic ice shelves that drain the AIS (Bronselaer et al., 2020; Purich & England, 2021; Spence et al., 2014, 2017).

The subpolar SO is a region where salinity dominates the stratification (Stewart & Haine, 2016) and is characterized by cold and fresh water in the upper few hundred meters that overlies warmer and saltier water at depth. This source of heat at depth makes the subpolar SO particularly important for regional and global climate change as changes in the local stratification can directly impact air-sea heat fluxes and alter the thermal properties of the waters that interact with the ice shelves. Antarctic meltwater increases stratification in the upper ocean which inhibits the upward vertical mixing of heat from the ocean interior and its release to the atmosphere. The subsurface ocean warms as a consequence of the reduced vertical heat transport (Bronselaer et al., 2018). Robust responses to increased Antarctic meltwater have been documented in modeling studies utilizing diverse methods for applying the meltwater forcing, differing background climatological states, and differing model resolutions (Bintanja et al., 2013; Bronselaer et al., 2018; Fogwill et al., 2015; Lago & England, 2019; Ma & Wu, 2011; Mackie et al., 2020; Menviel et al., 2010; Moorman et al., 2020; Pauling et al., 2016; Purich et al., 2018; Sadai et al., 2020; Snow et al., 2016; Stouffer et al., 2007; Swart & Fyfe, 2013; Swingedouw et al., 2009). Common responses reported in all of the studies cited above include a strong cooling of surface air temperature (SAT) and sea surface temperature (SST), expansion and thickening of Antarctic sea ice, reduced Antarctic Bottom Water (AABW) formation, increased subsurface heat content, and shifts in global wind and precipitation patterns (Bronselaer et al., 2018; Ma & Wu, 2011; Mackie et al., 2020; Stouffer et al., 2007; Swingedouw et al., 2009).

Most of these studies have utilized intermediate complexity models (Golledge et al., 2019; Menviel et al., 2010; Swart & Fyfe, 2013; Swingedouw et al., 2009) or fully coupled climate models with coarse horizontal grid spacing ocean components ($\geq 1°$; Bintanja et al., 2013; Bronselaer et al., 2018, 2020; Fogwill et al., 2015; Ma & Wu, 2011; Pauling et al., 2016; Purich et al., 2018; Sadai et al., 2020; Stouffer et al., 2007). Given that wind and meltwater forcing in the SO elicit a complex response involving feedbacks between atmospheric, oceanic, and sea-ice processes through the disruption of large-scale circulation systems, full model coupling is critical. However, small-scale features in ocean circulation, which are not resolved at the grid spacing of most coupled climate models ($\sim 1°$), including submesoscale and mesoscale eddies and narrow coastal boundary currents, play a fundamental role in SO circulation and feedbacks between the open ocean and the Antarctic shelf (Dinniman et al., 2016; Goddard et al., 2017; Stewart & Thompson, 2015; Stewart et al., 2019). At the latitudes where the Antarctic continental slope is located, the horizontal grid spacing required to resolve mesoscale eddies is generally finer than 5 km and even much finer than 1 km in regions on the shelf (Hallberg, 2013).

Experiments imposing individual wind or meltwater perturbations that have been performed using fine resolution models have been limited to global ocean sea-ice models (Lago & England, 2019; Moorman et al., 2020; Spence et al., 2014, 2017; Waugh et al., 2019, 2021) or high-resolution sector models (Snow et al., 2016). The utilization of global ocean sea-ice models or sector models, however, limits the ability to explore the fully coupled climate system response. Comparing the results between coarse and fine resolution ocean models reveals an interesting discrepancy in the response of shelf properties to increases in Antarctic meltwater. Coarse-resolution modeling results suggest that surface freshening from the additional meltwater enhances stratification in the upper water column, which (a) suppresses SO overturning, reduces the upward vertical mixing of heat (Bronselaer et al., 2018; Fogwill et al., 2015; Golledge et al., 2019; Menviel et al., 2010; Sadai et al., 2020) and (b) draws in more relatively warm offshore CDW, along isopycnals, onto the continental shelf (Bronselaer et al., 2018). These

21699291, 2022, 5, Downloaded from https://agupubs.onlinelibrary.wiley.com/doi/10.1029/2021JC017608 by University Of St Andrews University, Wiley Online Library on [08/11/2022]. See the Terms and Conditions (https://onlinelibrary.wiley.com/terms-and-conditions) on Wiley Online Library for rules of use; OA articles are governed by the applicable Creative Commons License

results suggest a positive feedback mechanism whereby additional meltwater can lead to enhanced subsurface warming along the shelf, which would act to increase basal melting of Antarctic ice shelves.

In contrast, studies utilizing finer resolution models suggest the thermal response along the Antarctic shelf to Antarctic meltwater is more nuanced in both space and time, with some shelf sectors experiencing increased warming and others experiencing strong cooling (Goddard et al., 2017; Moorman et al., 2020; Snow et al., 2016). In particular, fine resolution modeling results suggest that subsurface waters along the West Antarctic shelf, where accelerated thinning of ice shelves is currently observed (Paolo et al., 2015; Shepherd et al., 2004; The IMBIE team, 2018), experience an initial transient warming followed by strong cooling (Moorman et al., 2020) in response to increased Antarctic meltwater. Strong subsurface cooling of West Antarctic shelf waters suggests the potential for a negative feedback mechanism that would act to limit further Antarctic ice loss in some locations. Given these conflicting results between simulations imposing meltwater perturbations in coarse and fine resolution models, how the Antarctic shelf region will respond to increased melt remains highly uncertain.

A key component that likely contributes to the above discrepancy is whether a model sufficiently resolves the Antarctic Slope Front (ASF) and its associated Antarctic Slope Current (ASC). Strong lateral density gradients exist between the cold and fresh waters on the Antarctic continental shelf and relatively warm and saline CDW in the open ocean. Along this gradient, the ASC transports water westward along the Antarctic continental slope in a near-circumpolar pattern (Jacobs, 1991; Thompson et al., 2018; Whitworth et al., 1998). The ASC acts as a dynamical barrier between the shelf waters and the subpolar open ocean, thus its structure and transport play a vital role in modulating the exchange of ocean properties, including heat, between the continental shelf and the rest of the global ocean (Heywood et al., 2014; Thompson et al., 2018). Previous work has highlighted that refined horizontal resolution is required for representing the ASC in models (Dufour et al., 2017; Lockwood et al., 2021; Matthiot et al., 2011; Stewart & Thompson, 2015), and models that resolve a realistically strong ASC retain more freshwater on the shelf compared to coarse resolution models whose ASC is weak or non-existent (Lockwood et al., 2021).

The ASC is sensitive to both wind and meltwater forcing. As the westerlies shift poleward, weakened surface easterly wind stress reduces the Ekman pumping over the Antarctic shelf. This reduced Ekman pumping then weakens the ASC, shoals isopycnals at the shelf break, and has been shown to lead to rapid warming of the shelf as CDW can more readily access these regions (Spence et al., 2014, 2017). By contrast, shelf freshening acts to increase the lateral density gradient between the shelf and open ocean, steepening the isopycnals at the shelf break, and accelerating the ASC (Goddard et al., 2017; Moorman et al., 2020; Snow et al., 2016). An enhanced ASC acts to isolate the Antarctic shelf from warm CDW intrusions. A natural question then is, which one of these processes will dominate in the future? How will the ASC evolve and what does this mean for cross-slope exchange of ocean properties and the future stability of the AIS?

In this study, we use two fully coupled global climate models at differing horizontal ocean grid spacings, GFDL-CM4 with a 0.25° nominal grid spacing (eddy-permitting) and GFDL-ESM4 at 0.50° (eddy-parameterized), to explore the response of the SO to increased Antarctic meltwater and changes in the Southern Hemisphere wind field under a preindustrial control state. The magnitude of the wind stress and meltwater forcing imposed are those that can be expected near the middle of the 21st century under a high-emissions scenario. Differing from previous studies (Bronselaer et al., 2018) that impose a uniform freshwater forcing along the entire Antarctic coastline, we distribute the meltwater in a more spatially realistic pattern based on patterns of observed ice shelf melt. Our wind stress forcing also improves upon the realism of previous studies by capturing seasonal and regional variations which have important implications for regional differences in the ocean response (Goyal et al., 2021; Waugh et al., 2021). We assess the response to these forcings focusing on the properties and circulation in the open ocean and along the Antarctic continental shelf, with a priority of understanding mechanisms and biases contributing to robust and diverging model responses to the perturbations.

2. Methods

2.1. Models Used

We use a coupled global climate model (CM4) and an Earth system model (ESM4), both developed at the Geophysical Fluid Dynamics Laboratory (GFDL) of the National Oceanic and Atmospheric Administration (NOAA). The ocean/sea-ice components of the two models are different configurations of the GFDL-OM4.0

21699291, 2022, 5, Downloaded from https://agupubs.onlinelibrary.wiley.com/doi/10.1029/2021JC017608 by University Of St Andrews University, Wiley Online Library on [08/11/2022]. See the Terms and Conditions (https://onlinelibrary.wiley.com/terms-and-conditions) on Wiley Online Library for rules of use; OA articles are governed by the applicable Creative Commons License

ocean/sea-ice model (Adcroft et al., 2019), mainly differing in their horizontal grid spacing and treatment of mesoscale eddies as described below. Both models share version six of the Modular Ocean Model (MOM6) configured with a hybrid vertical ocean coordinate as facilitated by MOM6's use of the vertical Lagrangian remapping method (Griffies et al., 2020). Specifically, CM4 and ESM4 employ a hybrid vertical coordinate with z^* (quasi-geopotential) coordinates in the upper ocean through the mixed layer, and transition to isopycnal (referenced to 2,000 dbar) coordinates in the ocean interior for a total of 75 vertical layers (Adcroft et al., 2019). Both models include a baroclinicly induced submesoscale eddy restratification parameterization (Fox-Kemper et al., 2011). The sea ice model is the Sea Ice Simulator version 2 (SIS2.0) which has five thickness categories and shares the same Arakawa C-grid as MOM6. The horizontal grid spacing of SIS2.0 is the same as that of the respective ocean grid for each model.

While these two models are similar in many regards, there are several key differences between CM4 and ESM4 that we will highlight next. Readers are referred to Adcroft et al. (2019), Held et al. (2019), Dunne, Horowitz, et al. (2020) for a more detailed description of model components. For a side-by-side comparison of component-level differences between the two 207 models, see Table 1 in Dunne, Horowitz, et al. (2020).

2.1.1. ESM4 Model Description

The ocean component of ESM4 is MOM6 with a nominal 0.50° Mercator horizontal grid spacing that transitions to a tripolar grid poleward of 65°N (~22 km grid spacing at 65°S and 17–13 km between 70° and 75°S where the Antarctic continental shelf and slope are located). A key difference in the ocean formulation of ESM4 is the inclusion of a parameterization of mesoscale eddies. Additionally, the baroclinicly induced submesoscale eddy restratification parameterization is based on a front length of 200 m in ESM4, leading to a stronger restratification effect compared to CM4. Readers are referred to Adcroft et al. (2019) for more details on configurations and differences in the mean-state ocean simulation in these two MOM6 configurations. ESM4 has enhanced sea ice and snow-on-glacier albedo compared to CM4. To maintain the opening of coastal polynyas around Antarctica and prevent interior oceanic heat buildup, the sea ice albedo was raised from 1 to 1.5 standard deviations of observational uncertainty and snow-on-glacier near-infrared albedo was increased to 0.82 in ESM4 (see Dunne, Horowitz, et al., 2020). The ocean component of ESM4 is fully coupled to the second generation of the Carbon, Ocean Biogeochemistry, and Lower Trophics model (COBALTv2; Stock et al., 2020) and the model can represent feedbacks between biogeochemical processes and the physical ocean.

The atmospheric component of ESM4 is AM4.1, which features enhanced vertical resolution and more complex representation of aerosols and atmospheric chemistry compared to CM4. The AM4.1 model has 49 levels, extending to a top level of 1 Pa (~80 km), with enhanced resolution in the stratosphere relative to AM4.0. The land model in ESM4 is LM4.1, an updated version of LM4.0 used in CM4 whose primary differences include improvements in the representation of hydrography and a new terrestrial vegetation scheme. See table 1 and the associated discussion in Dunne, Horowitz, et al. (2020) for details on the significant updates in the AM4.1 and LM4.0 model components used in ESM4 relative to those in CM4. Also, see Horowitz et al. (2020) for a more in-depth presentation of the new version of the atmosphere component.

2.1.2. CM4 Model Description

The ocean component in CM4 has a nominal 0.25° Mercator horizontal grid spacing that transitions to a tripolar grid poleward of 65°N (~11 km grid spacing at 65°S and ~9–7 km between 70° and 75°S where the Antarctic continental slope and shelf are located). CM4 has no mesoscale eddy parameterization in the ocean and is considered an "eddy-permitting" model. At 0.25° grid spacing, transient eddies are present in the simulation in the tropical and subtropical oceans, yet incompletely resolved at higher latitudes. The baroclinic Rossby deformation radius is ~4 km near the Antarctic shelf (Hallberg, 2013), thus the CM4 grid spacing is insufficient to resolve the mesoscale eddy field on and near the Antarctic shelf. The baroclinicly induced submesoscale eddy restratification parameterization is based on a front length of 500 m in CM4. The ocean model is coupled to the reduced-complexity global Biogeochemistry with Light, Iron, Nutrients, and Gas model version 2 (BLINGv2; Dunne, Bociu, et al., 2020) to represent nutrient cycling and carbonate chemistry, however in CM4, BLINGv2 is purely diagnostic and ocean color is prescribed.

The atmospheric component of CM4 is the GFDL Atmospheric Model version 4.0 (AM4.0) described in Zhao et al. (2018a, 2018b), with ~100 km horizontal grid spacing (C96; 96 × 96 grid boxes on each of the six cube-sphere faces) and 33 levels in the vertical that extend to 100 Pa (~45 km). The land component is the

21699291, 2022, 5, Downloaded from https://agupubs.onlinelibrary.wiley.com/doi/10.1029/2021JC017608 by University Of St Andrews University, Wiley Online Library on [08/11/2022]. See the Terms and Conditions (https://onlinelibrary.wiley.com/terms-and-conditions) on Wiley Online Library for rules of use; OA articles are governed by the applicable Creative Commons License

GFDL Land Model Version 4.0.1, which is an updated version of the land model from that described in Zhao et al. (2018a, 2018b).

2.2. Experimental Design

2.2.1. Wind Stress and Antarctic Meltwater Perturbations

The goal of this study is to isolate the physical response of the ocean and climate system to CO_2-forced changes in surface wind stress forcing, meltwater input from the AIS, and the combined forcing of the two. Hereafter we refer to these three experiments as Stress, Antwater, and AntwaterStress, respectively (Table A1) All simulations are initialized as a step-perturbation branching from the previously spun-up preindustrial control (piControl) integrations that were performed as part of the sixth phase of the Coupled Model Intercomparison Project (CMIP6; Eyring et al., 2016).

Following the Flux-Anomaly-Forced Model Intercomparison Project (FAFMIP; Gregory et al. (2016)) protocol, the Stress simulations impose a zonal and meridional momentum flux perturbation at the ocean surface (Figures 1c and 1d). In FAFMIP, all surface flux perturbations are derived from an ensemble-mean of 13 CMIP5 idealized 1pctCO_2 simulations, where atmospheric CO_2 concentrations are increased at a rate of 1% year^{-1} in a piControl state. The wind stress perturbation fields are taken from years 61 to 80 in the 1pctCO_2 simulations which are centered around the time of CO_2 doubling. Thus, the perturbation in the Stress experiments corresponds to expected changes in response to atmospheric CO_2 concentrations likely to be reached by middle of the 21st century under the high emission scenarios used in CMIP5 and CMIP6, Representative Concentration Pathway 8.5 (RCP 8.5; Riahi et al., 2011) and Shared Socio-economic Pathway 5-8.5 (SSP5-8.5; Meinshausen et al., 2020). The momentum perturbation results in an 8%–9% increase in the magnitude of the annual-mean zonally averaged maximum westerly wind stress and a ∼1° poleward shift over the SO (Figures 1c–1e).

The Antwater experiments impose a time-uniform 0.1 Sv freshwater transport entering the ocean surface and assumed to be at the SST. The freshwater is input in a one-degree latitude band in regions of observed ice shelf or ice sheet melting following observations in Paolo et al. (2015) and The IMBIE team (2018). The total freshwater perturbation is 0.1 Sv, but the contribution from each region is weighted based on observations (Figures 1a and 1b). Most of the freshwater input occurs in the Pacific sector, with the Amundsen-Bellingshausen (120°–70°W) and Ross (150°E−120°W) Seas amounting to 42% and 24%, respectively, of the total freshwater flux. The Weddell (70°W–0°), Indian (0°–80°E), and West Pacific (80°E–150°W) regions contribute 25%, 0.7%, and 9%, respectively. The 0.1 Sv freshwater transport perturbation is large relative to the observed estimate of AIS mass change of ∼0.0035 ± 0.0018 Sv (−109 ± 56 Gt yr^{-1}) averaged over the 1992–2017 period (The IMBIE team, 2018). However, a 0.1 Sv freshwater transport from the AIS is consistent with the total meltwater flux expected near mid-century under the RCP8.5 scenario, as determined from dynamic ice-sheet model simulations (DeConto & Pollard, 2016). Thus, because RCP8.5 mid-century atmospheric CO_2 concentrations (∼570 ppm) are approximately doubled relative to preindustrial values, the 0.1 Sv meltwater forcing pairs well with the Stress perturbations which were obtained from the transient response to atmospheric CO_2 doubling. The uncertainty in projected meltwater from the AIS over the course of the 21st century is large and the DeConto and Pollard (2016) estimate is at the upper end of the projected Antarctic melt expected by mid-century, yielding 0.04 m of Antarctic contribution to sea level rise by year 2050 under RCP8.5 compared to 0.02–0.03 m estimated in other studies (see table 4.3 of Oppenheimer et al. (2019)). The AntwaterStress experiment applies both the wind stress and meltwater perturbations simultaneously. This AntwaterStress experiment employs the same forcings as the "Antwater-Stress" experiment listed under the FAFMIP protocol, however for clarity, we omit the "-" so as not to be incorrectly interpreted as "Antwater minus Stress."

Both models exhibit centennial-scale variability that occurs in the SO due to open ocean convective events in the Ross Sea that are characteristic of both models (Dunne, Horowitz, et al., 2020; Held et al., 2019). Due to this internal-variability, multiple-ensemble members are run for each experiment to help differentiate signal from noise. The branch points from the piControl for the three ensemble members were chosen to sub-sample the magnitude of the subsurface heat reservoir in the Ross Sea which is dynamically linked to the large-scale polynya events characteristic to both models (Figure A1). This design choice results in an ensemble member with a 70-year period in which there was no polynya event in the corresponding piControl integration, a member that is initialized ∼40 years prior to large polynya event, and a member initialized at the start of a polynya. Since these

21699291, 2022, 5, Downloaded from https://agupubs.onlinelibrary.wiley.com/doi/10.1029/2021JC017608 by University Of St Andrews University, Wiley Online Library on [08/11/2022]. See the Terms and Conditions (https://onlinelibrary.wiley.com/terms-and-conditions) on Wiley Online Library for rules of use; OA articles are governed by the applicable Creative Commons License

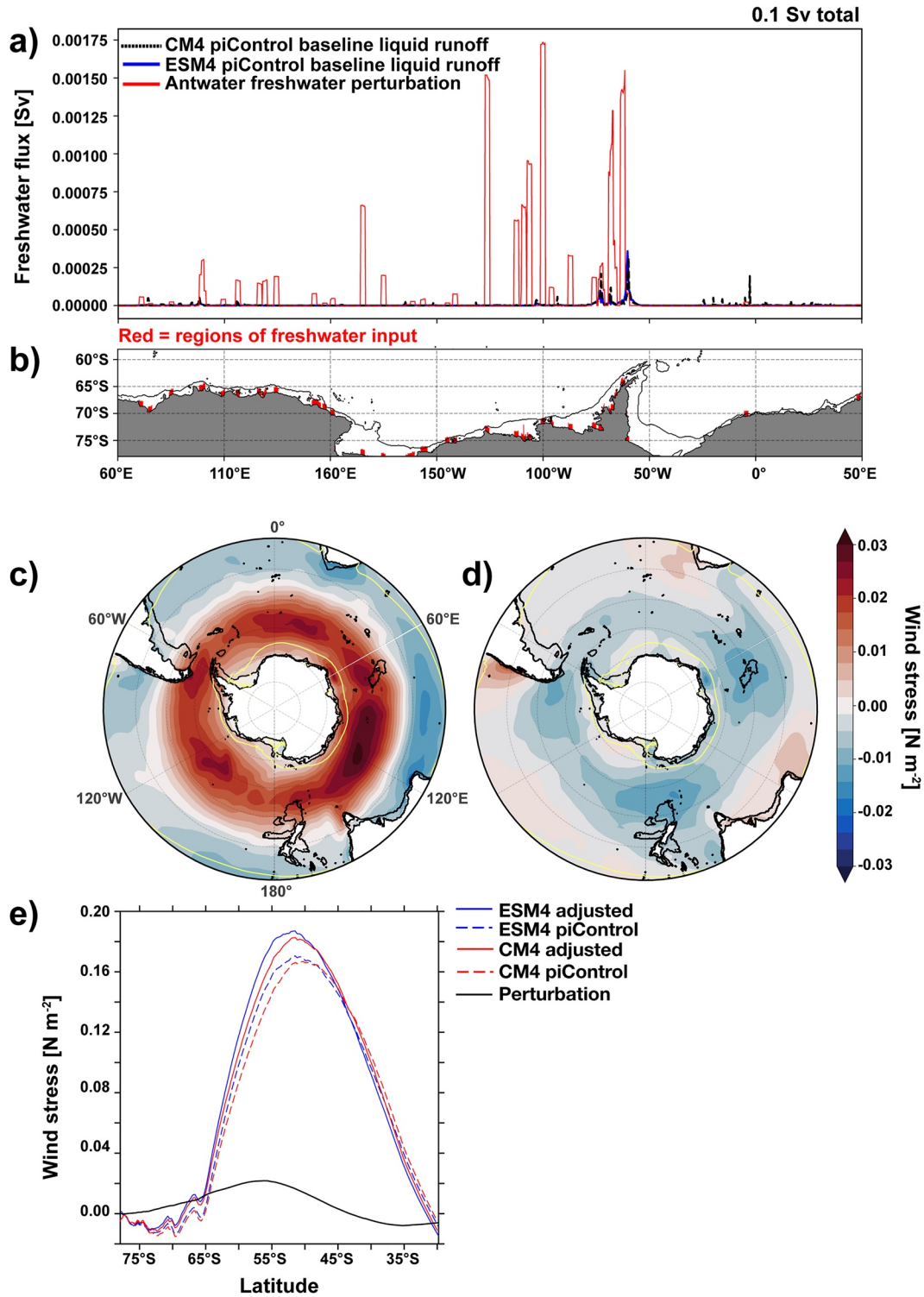

Figure 1. (a) Magnitude and (b) spatial pattern of freshwater input (Sv) around the Antarctic coast implemented in the Antwater and AntwaterStress experiments. The baseline annual-mean liquid runoff entering at the Antarctic coast for CM4 and ESM4 is shown in panel (a) for comparison to the meltwater perturbation. (c) Zonal and (d) meridional wind stress (N m^{-2}) perturbation applied in the Stress and AntwaterStress experiments. (e) Original and adjusted zonal-mean zonal wind stress (N m^{-2}) over the Southern Ocean for CM4 and ESM4. The 1,000 m isobath next to the Antarctic continent is contoured in black and the zero wind stress line, that is, where the zonal wind stress transitions from westerlies to easterlies is contoured in yellow in the polar projections.

21699291, 2022, 5, Downloaded from https://agupubs.onlinelibrary.wiley.com/doi/10.1029/2021JC017608 by University Of St Andrews University, Wiley Online Library on [08/11/2022]. See the Terms and Conditions (https://onlinelibrary.wiley.com/terms-and-conditions) on Wiley Online Library for rules of use; OA articles are governed by the applicable Creative Commons License

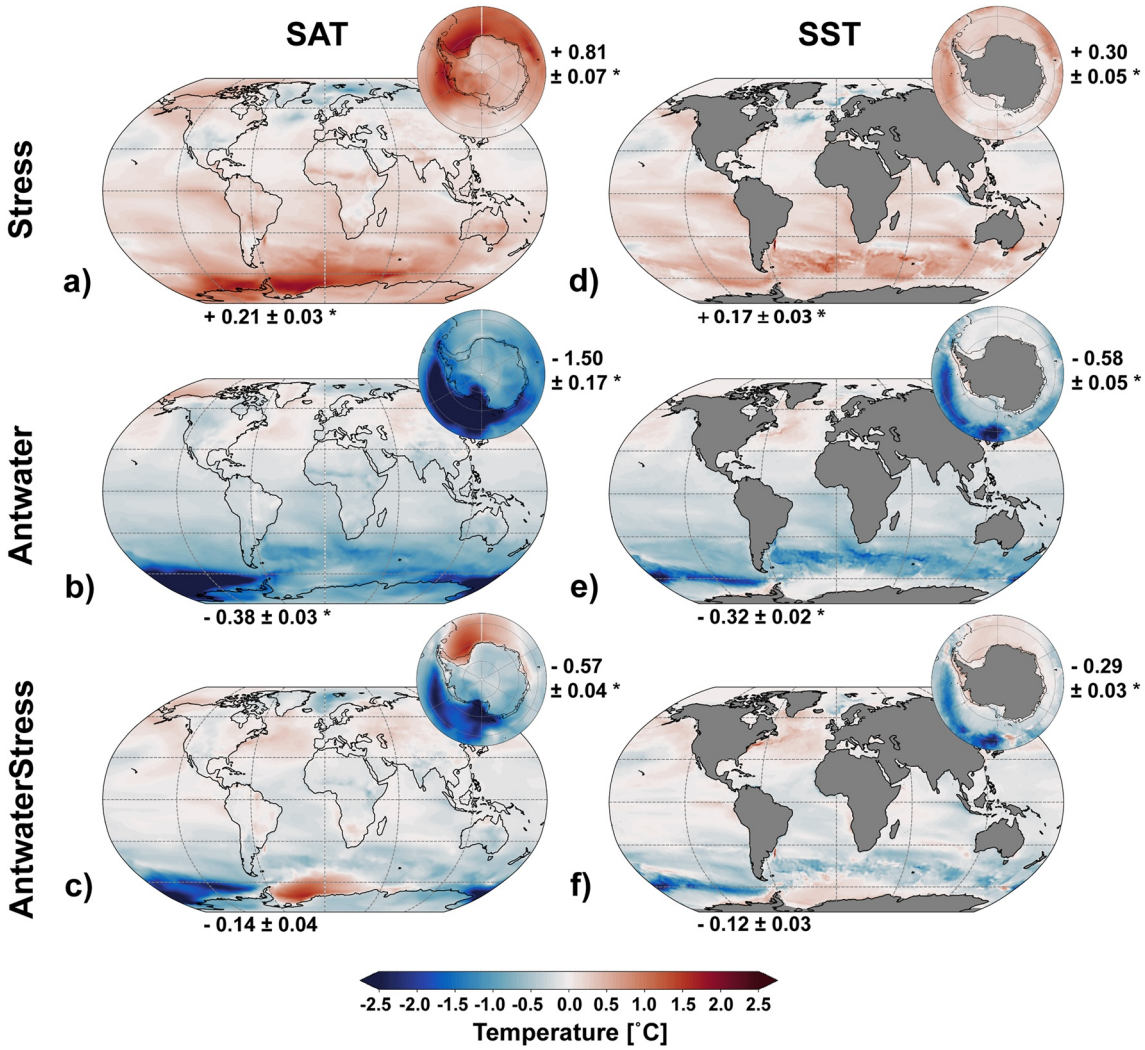

Figure 2. (a–c) Ensemble-mean annual-mean surface air temperature (SAT; °C) and (d–f) sea surface temperature (SST; °C) response in CM4. Changes in the global-mean properties and properties south of 55°S (northern boundary of inset polar projections) with the ensemble spread (1σ) are shown at the bottom left and top right of each panel, respectively. Values marked with an asterisk (*) are greater than 2σ outside of the piControl long-term average. The 1,000 m isobath is contoured in each polar projection, representing the boundary between the shelf and open ocean. Dashed latitude lines are shown in each polar projection at intervals of 10° from 70° to 60°S, with the northern boundary located at 55°S.

simulations span ranges that capture different phases of SO variability, all differences are computed between the last 20 years of the perturbation experiment (years 51–70) and a 100-year average in the piControl integration (perturbation – piControl). The 100-year period in the piControl is chosen to overlap with the integrations for all ensemble members. Unless otherwise noted, all results are analyzed as the ensemble-mean response.

3. Results

3.1. Surface Temperature Response

A robust response in Southern Hemisphere surface temperature properties is found across ensemble members in both CM4 and ESM4 (Figures 2 and 3). In the SO, this response is characterized by strong SAT and SST warming in Stress and strong cooling of SAT and SST in Antwater. In Stress, the greatest SAT warming occurs in the Amundsen-Bellingshausen Seas, the Weddell, and the South Indian Ocean. The SST response shows a more circumpolar pattern, with maximum warming occurring between 60° and 30°S. The differing SAT and SST patterns suggest a redistribution of heat, where the Stress perturbation drives ocean heat release in the subpolar

21699291, 2022, 5, Downloaded from https://agupubs.onlinelibrary.wiley.com/doi/10.1029/2021JC017608 by University Of St Andrews University, Wiley Online Library on [08/11/2022]. See the Terms and Conditions (https://onlinelibrary.wiley.com/terms-and-conditions) on Wiley Online Library for rules of use; OA articles are governed by the applicable Creative Commons License

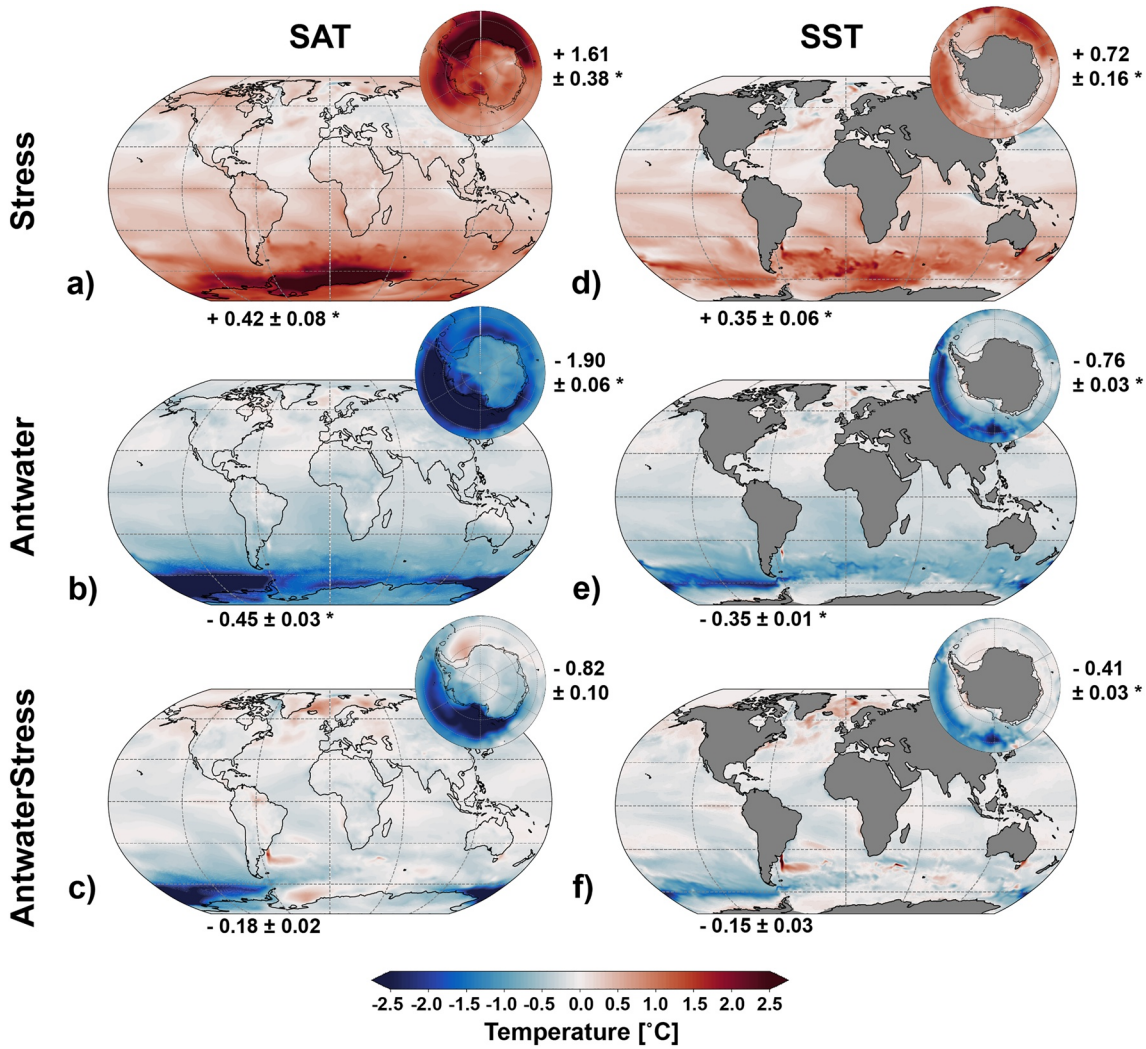

Figure 3. Same as Figure 2, but for the ESM4 simulations.

SO and heat uptake at midlatitudes in regions where intermediate and mode-waters are formed and subducted. The magnitude of SAT and SST warming in ESM4 is approximately double that in CM4.

In Antwater, the greatest SAT cooling in the SO occurs in the South Pacific. More SAT cooling occurs throughout the Weddell Sea in ESM4 compared to CM4, with ESM4 exhibiting strong cooling anomalies adjacent to the shelf in the southern sector of the Weddell Gyre. The SST response in Antwater is circumpolar in nature, with the largest change in SST occurring north of 60°S. This cooling is likely a result of delivery of the cold and fresh meltwater to the midlatitudes through sea ice processes and advection of freshwater northward in the South Atlantic by the Antarctic Circumpolar Current (ACC). Similar to the response in Stress, ESM4 yields a greater degree of surface cooling relative to CM4.

In AntwaterStress, there is a strong cooling in the Amundsen-Bellingshausen and Ross Seas and a warming in the South Atlantic, mostly concentrated in the Weddell Sea. While the meltwater dominates the response, the warming in the South Atlantic mediates the signal, resulting in ∼38% and 43% less SAT cooling compared to the Antwater experiments in CM4 and ESM4, respectively. Again, ESM4 shows a larger response to the perturbations in AntwaterStress, with a greater cooling in the subpolar SO and only a slight warming in the Weddell Sea. Importantly, the surface response in AntwaterStress is not a simple linear combination of the Antwater and Stress temperature anomalies; however, the degree of nonlinearity differs between the models, with a more nonlinear response in ESM4 (Figure A2).

21699291, 2022, 5, Downloaded from https://agupubs.onlinelibrary.wiley.com/doi/10.1029/2021JC017608 by University Of St Andrews University, Wiley Online Library on [08/11/2022]. See the Terms and Conditions (https://onlinelibrary.wiley.com/terms-and-conditions) on Wiley Online Library for rules of use; OA articles are governed by the applicable Creative Commons License

In all three experiments, the signals are strongest south of 55°S; however, the impacts extend beyond the SO. In the Antwater and Stress experiments, significant changes (2σ outside of the piControl long-term average) are found in global mean SAT and global mean SST. For both models, robust spatial patterns and similar magnitudes of SAT and SST anomalies are found in the Southern Hemisphere across ensemble members for all experiments (individual members not shown here). However, the anomalies in the Northern Hemisphere, specifically north of 30°N are less robust across ensemble members in both models. The larger ensemble spread in the surface temperature response in the Northern Hemisphere is not surprising given the freshwater perturbation is only applied in the SO and the largest surface wind stress anomalies occur in the Southern Hemisphere. In general, the meltwater perturbation dominates the global SAT and SST response in the AntwaterStress experiments. We propose that the meltwater dominates the global response since the addition of meltwater acts in one direction in the open ocean—to trap oceanic heat through increased stratification (decreased ventilation) and enhanced sea ice extent. The changes in wind stress induce competing effects on the heat budget: acting as a "release valve" on oceanic heat in the subpolar SO while simultaneously acting to trap heat within the ocean at midlatitudes. The dominance of the meltwater signal may also stem from the fact that, if we consider the percentage change relative to the baseline forcing, the meltwater addition is more sizable than the change in the surface wind stress.

3.2. Sea Ice Response and Polynya Generation

In the Stress experiments, there is a contraction in the maximum winter and summertime sea ice extent (SIE; not shown) in both models accompanied by sea ice thinning (Figures 4a and 4d), with the greatest change occurring in the South Atlantic and Indian Oceans co-located with regions of strong SAT and SST anomalies (Figures 2 and 3). The response for both fields is larger in ESM4. The reduction in sea ice thickness and fraction coincides with a drop in surface albedo (not shown), helping to sustain the surface warming. This adjustment of the sea ice to the wind stress perturbation occurs rapidly, within the first ∼10 years of the simulation.

The diminished sea ice state, in combination with the magnitude of the mean-state subsurface ocean heat reservoir, pre-condition the subpolar SO for the occurrence of large open ocean polynyas (Figure 5). Open ocean polynyas lead to further SAT warming in the Stress simulations as the open ocean is exposed to cold winter-time air, causing intense heat fluxes from the ocean to the atmosphere. In both models, most of the Weddell Sea polynya events that occur in the Stress simulations are initiated near the Maud Rise oceanic plateau, where polynyas have been observed in nature (Campbell et al., 2019; Cheon & Gordon, 2019; Gordon, 1978). These initially localized events eventually lead to near-complete wintertime sea ice loss in ESM4 in the Queen Maud region, exposing large swathes of the open ocean to the cold winter atmosphere for several years. The magnitude and extent of convection and concurrent heat release by these polynya events are likely tied to the mean-state subsurface heat reservoir available in the subpolar SO at the initialization point of each ensemble member (Figure A1).

The response of sea ice in the Antwater experiments is consistent with previous studies, whereby a freshening of the surface ocean leads to an enhancement of SIE and sea ice thickness (Figures 4b and 4e). The region of greatest thickening and expansion occurs in the South Pacific where most of the meltwater enters the ocean. The additional freshwater not only increases stratification in the upper ocean and reduces the upward vertical transfer of heat from below, but also raises the seawater freezing point to thus allow for more sea ice formation. We are thus led to a positive feedback whereby enhanced sea ice promotes further SAT cooling, producing conditions more conducive for further sea ice expansion and thickening. ESM4 shows a relatively uniform pattern of sea ice thickening in the open ocean and on the shelf. CM4 shows an inhomogeneous response, particularly in the Weddell Sea where a slight thinning occurs in the open ocean and a thickening is found on the shelf. Despite being statistically insignificant (within 2σ of the piControl long-term average), this weak thinning in the Weddell Sea is robust across all the CM4 Antwater ensemble members, suggesting it is a forced response. In both models, the additional surface freshening prevents open ocean polynyas from occurring in both the Weddell and Ross Seas (Figure 5).

The AntwaterStress sea ice response matches that of SAT and SST (Figures 2 and 3), with expansion and thickening in the South Pacific but of a lesser magnitude than Antwater and thinning in the Weddell Sea (Figures 4c and 4f). In both models, the freshwater perturbation dominates the response and prevents open ocean polynyas from forming in the Ross Sea. The models differ in that Weddell Sea open ocean polynyas continue to occur in CM4 despite the meltwater perturbation, yet they cease in ESM4 (Figures 5a and 5b).

21699291, 2022, 5, Downloaded from https://agupubs.onlinelibrary.wiley.com/doi/10.1029/2021JC017608 by University Of St Andrews University, Wiley Online Library on [08/11/2022]. See the Terms and Conditions (https://onlinelibrary.wiley.com/terms-and-conditions) on Wiley Online Library for rules of use; OA articles are governed by the applicable Creative Commons License

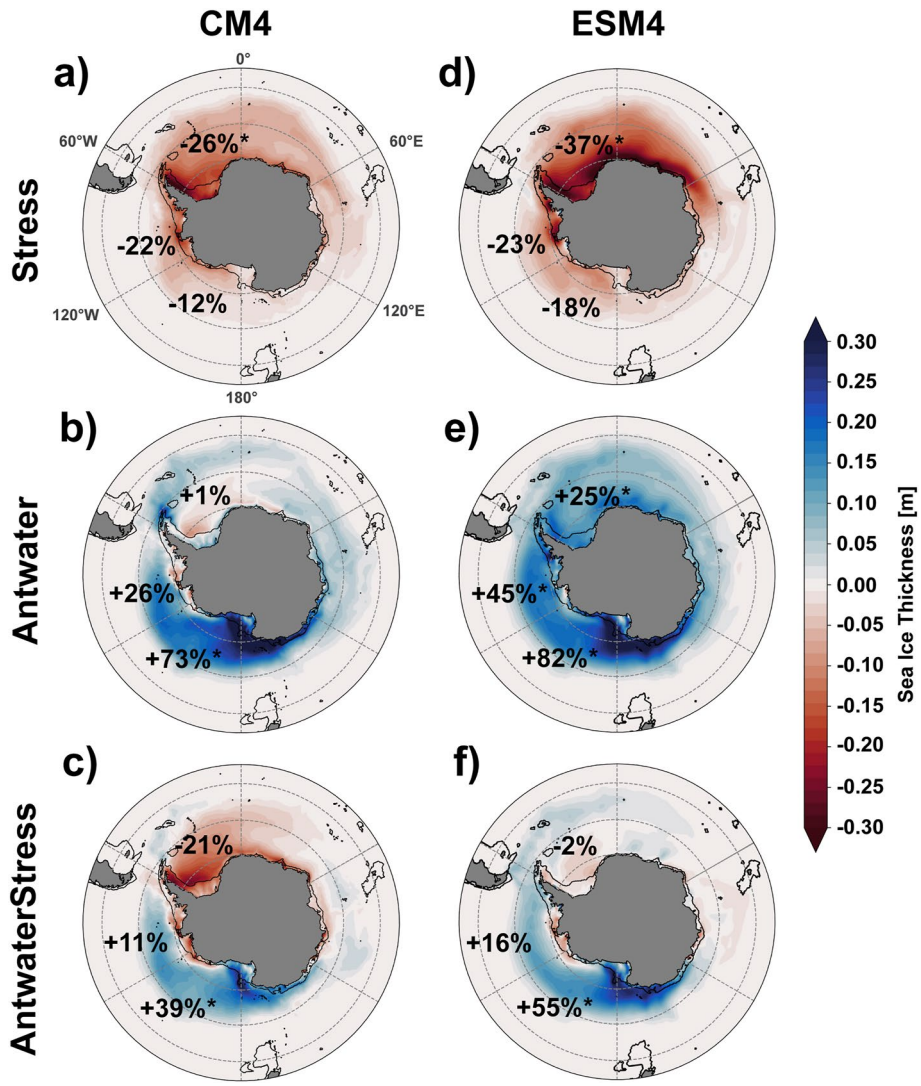

Figure 4. Ensemble-mean response of sea ice thickness (SIT; m) in CM4 and ESM4. Red indicates reduced SIT and blue indicates increased SIT. The percent change (%) in SIT in the Weddell (65°W to 0°), Amundsen-Bellingshausen (120° to 65°W), and Ross sectors (150°E to 120°W) are reported on each panel. Values marked with an asterisk (*) are regions where the change in SIT is greater than 2σ away from the piControl long-term average. The 1,000 m isobath is contoured, representing the boundary between the shelf and open ocean. Dashed latitude lines are shown at intervals of 10° from 70° to 50°S, with the northern boundary of each projection located at 45°S.

3.3. Subsurface Ocean Response

3.3.1. Open Ocean

We define the boundary between the open ocean and the shelf as the 1,000 m isobath (Goddard et al., 2017; Moorman et al., 2020). The open ocean (equatorward of the 1,000 m isobath) subsurface temperature and salinity (200–1,000 m depth-averaged) response to the Stress perturbation is similar between the two models yet more pronounced in ESM4 (Figures 6e–6h). Subsurface salinity shows minimal change in the subpolar SO in both models while the temperature response diverges. Strong cooling is found in the Weddell and Ross Seas in ESM4 (Figure 6h) that is not found in CM4. Both models show salinification and warming north of and within the latitude bands of the ACC (~55° – 50°S). The strongest magnitudes of subsurface warming and salinification occur in regions where the southward penetrating western boundary currents bring warm and saline subtropical waters into the SO and surface waters are transformed into intermediate and mode waters. These spatial patterns are likely the combined effect of a poleward shift of the subtropical gyre boundary in response to the poleward shift

21699291, 2022, 5, Downloaded from https://agupubs.onlinelibrary.wiley.com/doi/10.1029/2021JC017608 by University Of St Andrews University, Wiley Online Library on [08/11/2022]. See the Terms and Conditions (https://onlinelibrary.wiley.com/terms-and-conditions) on Wiley Online Library for rules of use; OA articles are governed by the applicable Creative Commons License

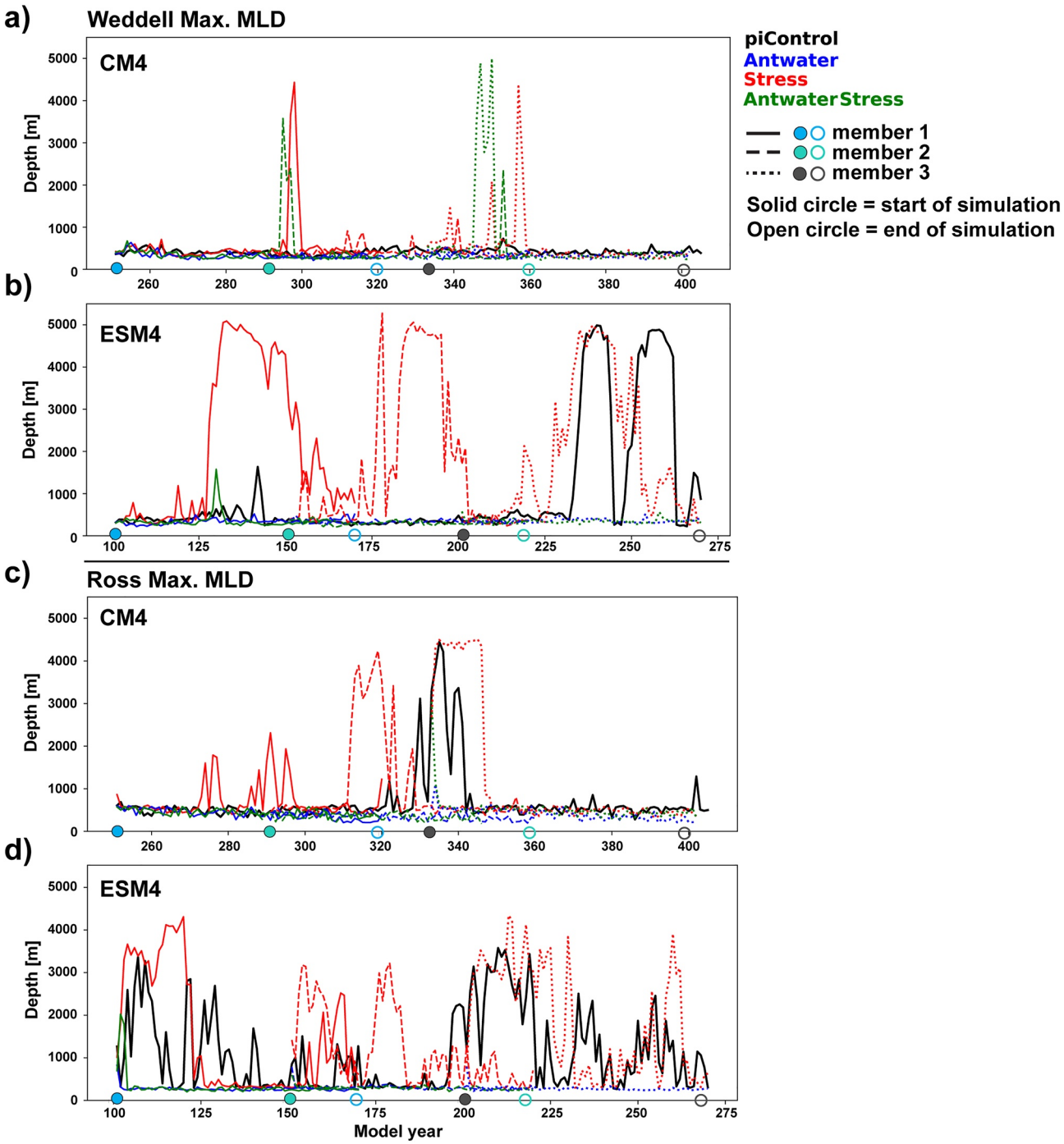

Figure 5. Maximum mixed layer depth (MLD; m) in the Weddell (a, b; 65°W to 0°) and Ross (c, d; 150°E to 120°W) sectors for each ensemble member and the respective piControl integration. The MLD is that used in the MOM6 mixed layer restratification parameterization, which is equivalent to the time-filtered energetic planetary boundary level depth (ePBL; Adcroft et al., 2019; Riechl & Hallberg, 2018). On the bottom of each panel, the start and end of each ensemble member are noted by the solid and open circles, respectively. The total time length shown for each member is 70 years.

in the westerly jet and the meridional redistribution of heat from the interior subpolar SO to midlatitudes, as the Stress perturbation enhances heat loss at high-latitudes through enhanced upwelling of CDW and triggering of polynya events (Figure 5; not shown, but cooling below 500–1,000 m is a robust feature across Stress ensemble members for each model). The pronounced subsurface cooling in the Weddell Sea in ESM4 (Figure 6h) is linked to the intense and extensive polynya events consistently triggered in this region (Figure 5b).

21699291, 2022, 5, Downloaded from https://agupubs.onlinelibrary.wiley.com/doi/10.1029/2021JC017608 by University Of St Andrews University, Wiley Online Library on [08/11/2022]. See the Terms and Conditions (https://onlinelibrary.wiley.com/terms-and-conditions) on Wiley Online Library for rules of use; OA articles are governed by the applicable Creative Commons License

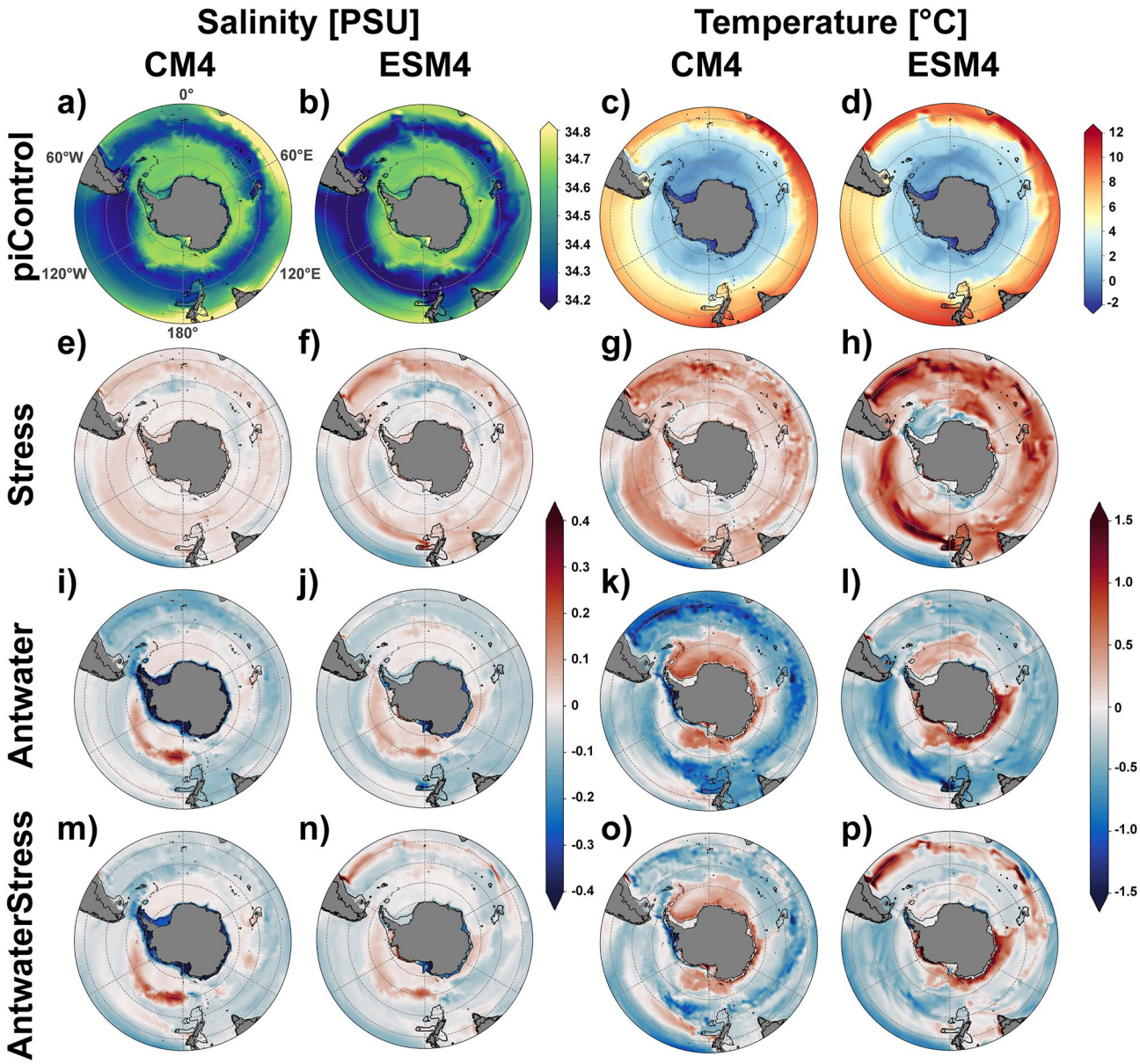

Figure 6. (a–d) 200–1,000 m depth-averaged piControl mean salinity (PSU; left two columns) and temperature (°C; right two columns) and ensemble-mean response (e–p) for each perturbation experiment. The 1,000 m isobath is contoured in each panel, representing the boundary between the shelf and open ocean. Dashed latitude lines are shown at intervals of 10° from 70° to 40°S, with the northern boundary of each projection located at 35°S.

The response in the Antwater experiments is more consistent between the two models (Figures 6i–6l). Increased salinity is found throughout most of the subpolar SO, with the strongest salinification in a coherent band in the South Pacific co-located with the region of most enhanced sea ice thickening and expansion (Figure 4). This band of enhanced salinity may be due to a northward shift in the outcrop location of fresh Antarctic Intermediate Water (AAIW) and more saline CDW in the upper ocean as the sea ice edge expands north. In the Weddell Sea, subsurface salinification occurs from the Antarctic coast to ∼50°S and enhanced freshening occurs to the north in regions of mode and intermediate waters. In CM4, the midlatitude freshening appears to emanate from the region where the ACC advects meltwater from West Antarctica into the South Atlantic (Figure 6i), with midlatitude fresh anomalies decreasing eastward from the Atlantic to the Pacific. The magnitude of the midlatitude fresh anomalies in ESM4 appears more homogenous (Figure 6j). The meltwater perturbation causes subsurface warming in the subpolar SO, with similar spatial patterns found between the models. However, ESM4 yields stronger warming adjacent to the shelf in the South Indian Ocean. Generally, the temperature response in the Weddell Sea

21699291, 2022, 5, Downloaded from https://agupubs.onlinelibrary.wiley.com/doi/10.1029/2021JC017608 by University Of St Andrews University, Wiley Online Library on [08/11/2022]. See the Terms and Conditions (https://onlinelibrary.wiley.com/terms-and-conditions) on Wiley Online Library for rules of use; OA articles are governed by the applicable Creative Commons License

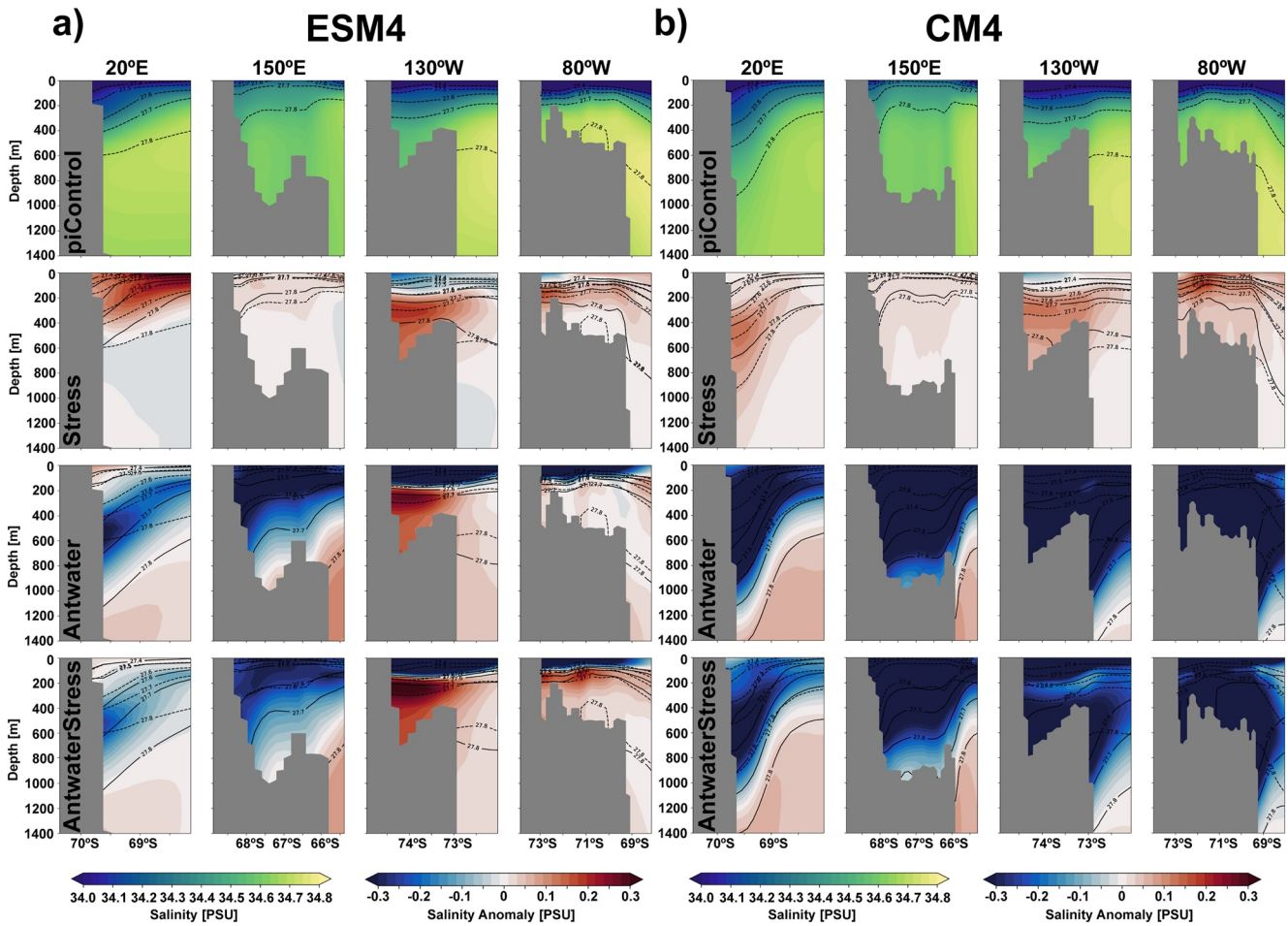

Figure 7. Ensemble-mean salinity (PSU) response along the Antarctic continental shelf at 20°E, 150°E, 130°W, and 80°W in (a) ESM4 and (b) CM4. The transects are the same regions where the ASC mean-state and response are assessed in Figures 9 and 10. Contours for potential density referenced to the surface are shown on each plot for the piControl simulation (dashed) and the last 20 years of the perturbation experiment (solid). The piControl mean salinity is shown in the top row.

mirrors that of salinity in both models. Opposite to the Stress response (Figures 6g and 6h), both models show strong cooling signals (Figure 6k-l) north of and within the latitude bands of the ACC (~55° – 50°S), likely from the incorporation of more cold water related to enhanced sea ice formation into the intermediate and mode waters formed in these regions.

The subsurface response in the AntwaterStress perturbations is consistent with the Antwater experiments in the subpolar South Pacific and South Indian sectors, yet the response in the Weddell Sea is slightly different (Figures 6m–6p). The largest signals of subsurface warming are adjacent to the shelf in CM4 with large portions of the Weddell Sea showing the minimal change. A thick layer of fresh and cold anomalies penetrates the upper 200–800 m of the subsurface layer in the ESM4 simulation, suggesting more incorporation of the fresh and cold meltwater into the open ocean. The temperature and salinity response at midlatitudes in the South Indian and South Atlantic in ESM4 in the AntwaterStress simulation is similar to the spatial patterns found in the Stress simulations (compare anomalies centered on ~50°S in Figures 6p and 6h), suggesting the Stress perturbation generally dominates the subsurface response at midlatitudes in ESM4.

3.3.2. Antarctic Shelf

The most striking difference between CM4 and ESM4 in their response to the perturbations are the changes in subsurface properties on the Antarctic shelf (region poleward of the 1,000 m isobath; Figures 6–8). In the Stress experiments, there is a general warming and salinification of the shelf found in both models (Figures 6–8). This warming is particularly prominent along the Marie Byrd Land sector (~130°W), where both models show

21699291, 2022, 5, Downloaded from https://agupubs.onlinelibrary.wiley.com/doi/10.1029/2021JC017608 by University Of St Andrews University, Wiley Online Library on [08/11/2022]. See the Terms and Conditions (https://onlinelibrary.wiley.com/terms-and-conditions) on Wiley Online Library for rules of use; OA articles are governed by the applicable Creative Commons License

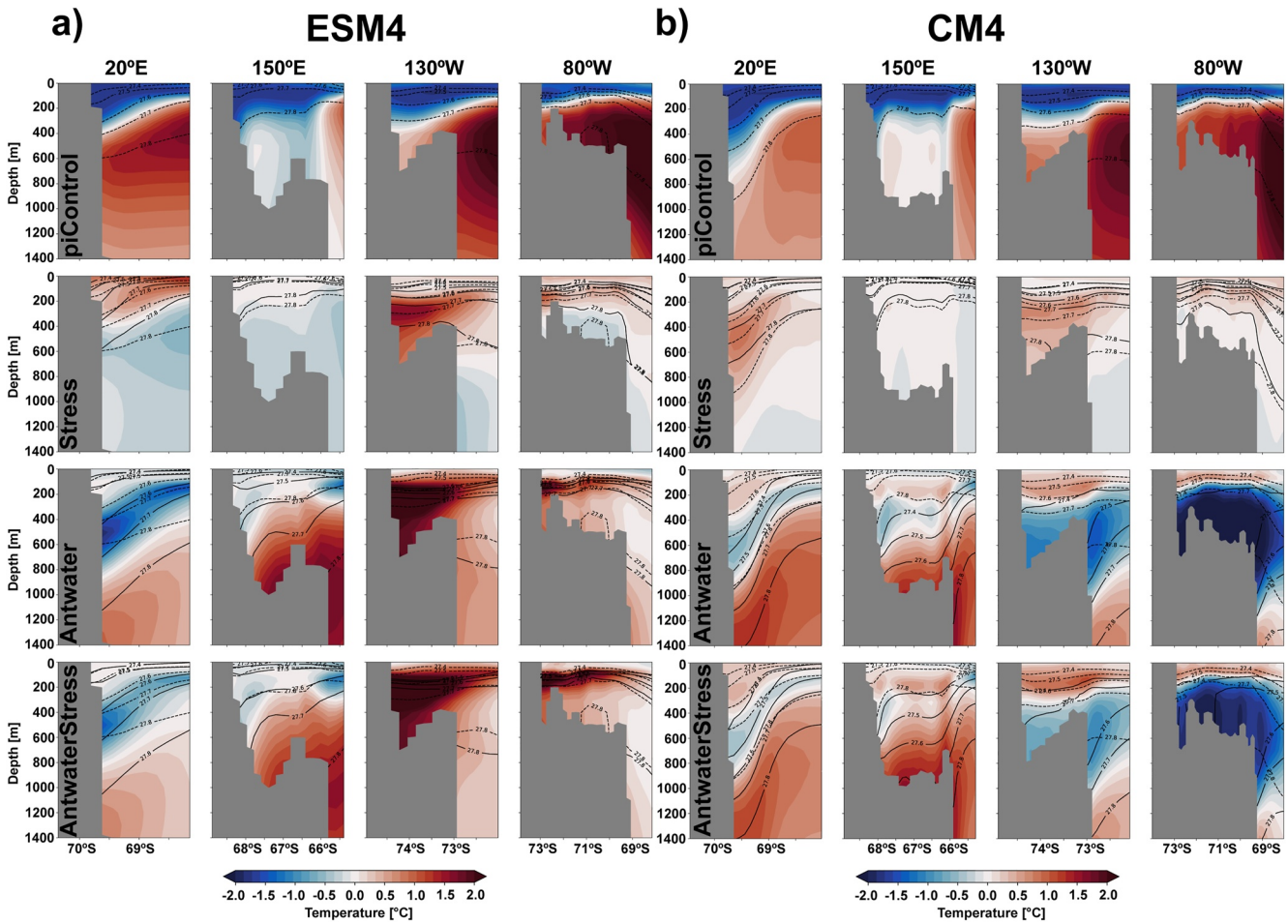

Figure 8. The same as Figure 7, but for temperature (°C). The color bar is the same for the piControl panels and the anomalies.

isopycnal shoaling and outcropping onto the shelf accompanied with strong warming (Figure 8). The spatial pattern of salinity and temperature change along the shelf is more homogenous in CM4. Along the WAP, CM4 shows a strong warming anomaly, while ESM4 shows slight cooling or little change. ESM4 also exhibits strong warming in the vicinity of the Amery Ice Shelf (~70°E) in the South Indian Ocean.

The meltwater perturbation clearly dominates the shelf response in the AntwaterStress experiments, producing nearly identical spatial patterns of temperature and salinity anomalies, but of slightly reduced magnitudes relative to the Antwater simulations in both models (Figures 6–8). There is a strong and spatially homogeneous freshening that is tightly constrained to the shelf in CM4 (Figure 6m). In ESM4, the spatial pattern of salinity anomalies is very inhomogeneous, with strong freshening on the shelf extending from the Ross Sea through the South Indian sector, slight freshening in the Weddell Sea and WAP, and salinification in the Amundsen-Bellingshausen Sea (Figure 6n).

The temperature change on the shelf in AntwaterStress is very inhomogeneous and yields different patterns between the two models. This difference is striking in West Antarctica, where CM4 shows a strong subsurface cooling extending from the WAP to ~130°W (Figure 6o) and ESM4 shows subsurface cooling along the tip of the Antarctic peninsula but strong subsurface warming westward until the Ross Sea (Figure 6p). The cross-sections at 130° and 80°W along the shelf highlight these differences (Figures 7 and 8). In CM4, these two sections show a layer of warming and freshening in the top 200 m, overlying an anomalously cold and fresh layer extending to the shelf floor. In ESM4, a thin layer of warming and freshening is found in the top 100 m that sits above anomalously warm and saline water. In CM4, the strong cooling and subsurface freshening in West Antarctica coincides with a decrease in ocean age (indicating recently ventilated water; Figure A3). The region of cooling around the

21699291, 2022, 5, Downloaded from https://agupubs.onlinelibrary.wiley.com/doi/10.1029/2021JC017608 by University Of St Andrews University, Wiley Online Library on [08/11/2022]. See the Terms and Conditions (https://onlinelibrary.wiley.com/terms-and-conditions) on Wiley Online Library for rules of use; OA articles are governed by the applicable Creative Commons License

tip of the WAP in ESM4 coincides with reduced ocean age, and the regions of strong subsurface warming with increased age (Figure A3). The continental shelf in the Weddell Sea shows little change in subsurface temperature and ocean age in both models under AntwaterStress. The lack of subsurface anomalies is linked to the fact that surface densification and the associated convection of surface-cooled waters persist on the Weddell shelf despite the additional freshening due to the meltwater perturbation. The minimal change in ocean age and temperature found in both models over the Weddell shelf is consistent with the results in Moorman et al. (2020).

3.4. Impacts on Open Ocean and Shelf Exchange

3.4.1. Response of the ASC

Prior to analyzing the response of the ASC, we provide a comparison of the mean-state representation of the ASC strength and structure in CM4 and ESM4. A robust assessment of a model's mean-state representation of the ASC is hindered by the fact that direct observations of the ASC are extremely sparse in space and time and the majority of existing observations of the velocity field are limited to "snap-shots" in time. Given the large spatial and temporal variability of the ASC shown in observations (Peña-Molino et al., 2016) and modeling studies (Huneke et al., 2022; Mathiot et al., 2011), assessing a model's mean-state performance against such snap-shots has the potential to be misleading. A 17-month transect of direct observations from a current meter moored array along the Antarctic continental slope in the southeastern Indian Ocean near 113°E (Peña-Molino et al., 2016) provides the only long-term (>1 year of sustained observations in a single location) benchmark to compare models against. However, even the Peña-Molino et al. (2016) observations are limited by the fact that the moorings only captured the full-time series of the flow below 500 m depth.

Owing to the paucity of direct long-term observations of ocean velocity along the continental slope and our desire to investigate the ASC mean-state and its response at various locations around the Antarctic shelf, we compare the piControl ASC to that simulated by the SO State Estimate (Mazloff et al., 2010) at 1/12° horizontal grid spacing for years 2006–2010. SOSE produces a physically realistic estimate of the ocean state in the SO by constraining a numerical ocean model by least-squares fit to all available ocean observations including that from Argo float profiles, shipboard CTD, mooring arrays, satellite sea surface height, instrument mounted seals, and so on (Mazloff et al., 2010). To test the suitability of using SOSE, we computed the transport below 500 m across the same 113°E transect observed over the 17-month period and reported by Peña-Molino et al. (2016). The total transport averaged over the full-time length of SOSE yields −17.7 Sv—slightly weaker than the observed transport of −19.3 ± 1.9 Sv, but with a velocity field generally consistent with that shown in Figure 5 of Peña-Molino et al. (2016).

In our assessment of the ASC strength in SOSE and the two models presented next, we do not differentiate between the Antarctic Coastal Current (ACoC), ASC, or the southern branches of the Weddell and Ross gyres but take the ASC to be the total vertically and horizontally integrated flow along the Antarctic continental margin at a particular longitude. Consistent with SOSE and direct observations (Thompson et al., 2018), the ASC develops and increases in strength westward from West Antarctica to the Weddell Sea in both models (Figure 9). The westward flow along the continental margin in the South Pacific and Southwest Indian, where the ASC is absent or weak, is similar between the two models, with magnitudes slightly weaker than SOSE's time-mean. The transport at 80°W differs between the models and SOSE, with the models simulating net eastward transport and SOSE yielding −8 Sv as a result of westward flow below 1,000 m. This pattern is similar to that in CM4; however, the deep westward component is much stronger in the SOSE, which may be the result of deep recirculations of the ACC that are better represented at higher resolution (Xu et al., 2020) or a better representation of the bottom intensified flow resulting from the overflow and subsequent downstream westward advection of DSW (Baines, 2009).

Where the ASC becomes well defined in the South Atlantic and Southeast Indian, the models differ from one another and CM4's strength and structure is more consistent with SOSE. At 20°E, the mean ASC in CM4 (−14 ± 6.8 Sv) is approximately double that of ESM4 (−7 ± 4.1 Sv). The strength of the ASC at 20°E in SOSE (−18 Sv) is slightly stronger than CM4. The ASC in CM4 is well defined and vertically sheared at 20°E in agreement with SOSE. These features are not found in ESM4, which instead has a weak and broad flow (Figure 9c). The circumpolar view of speed around the Antarctic continent shows that CM4 has a stronger and more well-defined ASC over the majority of continental slope (compare the high-speed magnitudes centered on the 1,000 m

21699291, 2022, 5, Downloaded from https://agupubs.onlinelibrary.wiley.com/doi/10.1029/2021JC017608 by University Of St Andrews University, Wiley Online Library on [08/11/2022]. See the Terms and Conditions (https://onlinelibrary.wiley.com/terms-and-conditions) on Wiley Online Library for rules of use; OA articles are governed by the applicable Creative Commons License

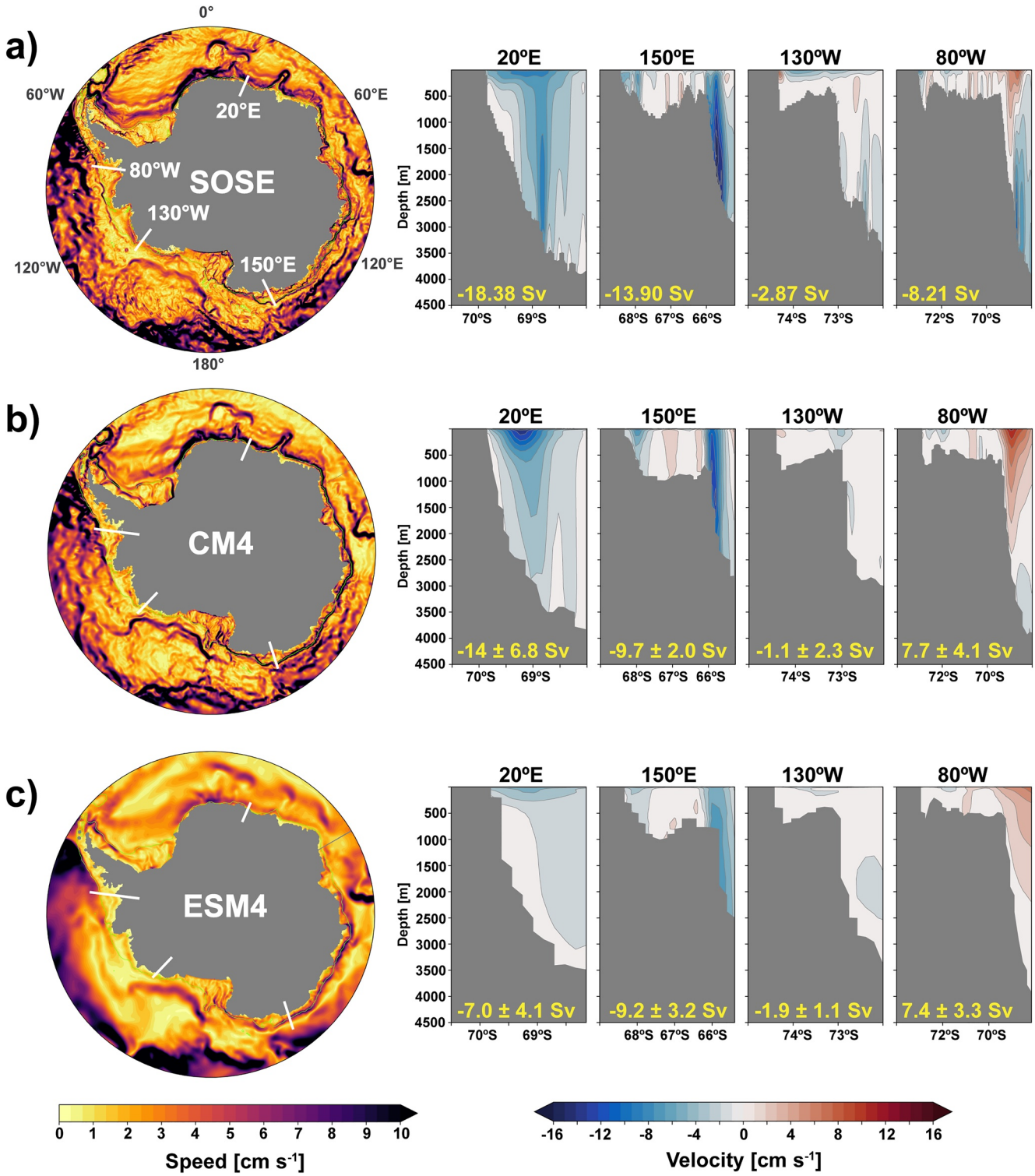

Figure 9. Speed (cm s^{-1}) depth-averaged over the upper 500 m and zonal velocity along the shelf and continental slope at four transects along the Antarctic coast (a) simulated in the 1/12°Southern Ocean State Estimate (SOSE) from 2006 to 2010 and (b)–(c) in the CM4 and ESM4 piControl simulations averaged over a 100-year period that overlaps with the perturbation experiments. The strength of the ASC is computed at four regions indicated by the white markers in each panel (20°E, 150°E, 130°W, 80°W). The mean strength for SOSE and the mean and interannual variability (1σ) for the 100-year period of the piControl simulation are listed in yellow on the velocity panels. For both speed and velocity, negative transports and velocities indicate net westward flow. Positive transports and velocities indicate net eastward flow. The 1,000 m isobath is contoured in green.

21699291, 2022, 5, Downloaded from https://agupubs.onlinelibrary.wiley.com/doi/10.1029/2021JC017608 by University Of St Andrews University, Wiley Online Library on [08/11/2022]. See the Terms and Conditions (https://onlinelibrary.wiley.com/terms-and-conditions) on Wiley Online Library for rules of use; OA articles are governed by the applicable Creative Commons License

isobath in Figures 9b and 9c). The spatial structure of speed around the Antarctic continent in CM4 is also consistent with that simulated by the ultra-fine LLC-4320 model with 1/48° horizontal grid -spacing (see figure 1 of Stewart et al. (2019)) which has been evaluated against existing (although sparse) direct observations. While the paucity of direct long-term observations prevents a sufficient evaluation of the mean-state ASC against that observed in nature, consistency with SOSE and the ultra-fine LLC-4320 model increase our confidence that the ASC strength and structure in CM4 are likely more consistent with reality compared to ESM4. In both models, there is a large degree of interannual to centennial-scale variability in the ASC present in their piControl simulations (Figure A4) related to local dynamics as well as the centennial polynya events in the Ross and Weddell Seas which disrupt lateral density gradients between the shelf and open ocean. We do not have adequate sustained observations or state estimates to investigate the realism of such ASC temporal variability.

We focus on ASC changes along the same sections where the shelf properties were assessed in Section 3.3 (Figure 10), which are also the same transects studied in Moorman et al. (2020). Consistent with the shelf anomalies, the meltwater perturbation dominates the ASC response in the AntwaterStress simulation at all sections, so we focus the discussion on the AntwaterStress results. There is a clear and near circumpolar acceleration of the westward flow along the 1,000 m isobath in CM4 with large increases at all locations (Figure 10a). The ESM4 simulation shows a general acceleration of the westward flow adjacent to the shelf, however, ESM4 is much weaker and more diffuse than in CM4 and it yields a reduction in westward flow at 150°E (Figure 10b).

A key difference between the two simulations is the response of the circulation along the WAP, a region that is dominated by eastward flow associated with the ACC in observations (Thompson et al., 2018) and in the piControl simulations (Figure 9). In CM4, a vertically sheared westward flowing current develops in this region, flowing from the Weddell through the Drake passage and along the WAP, reversing the transport from ∼8 Sv eastward to ∼7 Sv of westward flow at 80°W (Figure 10a). This behavior agrees with the establishment of sharp downward sloping isopycnals along the shelf-break (Figures 7 and 8). A sharp downward plunge of isopycnals toward the shelf is also found at 130°W (Figures 7 and 8) where the flow in CM4 increases by over 10 times its piControl strength. In ESM4, the eastward flow at 80°W weakens and moves further offshore, associated with a weakening ACC, however, no eastward current develops (Figure 10b). As a result of the increased sea surface height due to the additional meltwater, the ACoC along the shelf also strengthens in both models (Figure 10).

3.4.2. ASC as a Dynamical Barrier

As mentioned previously, there is large temporal variability of the ASC in the piControl simulations of both models (Figure A4). Examining total mass on the shelf, average shelf salinity, and the strength of the ASC throughout a 500-year segment of each models' piControl simulation reveals strong correlations between these measures (Figures 11a, 11b, 11d, and 11e). Time periods when the ASC is strong are associated with increased shelf mass and decreased shelf salinity. The total freshwater input over the shelf throughout the piControl simulations does not show this temporal variability suggesting that the ASC itself is acting as a strong control on the shelf salinity. When the ASC accelerates in the piControl simulations, the open ocean to shelf exchange becomes limited, and more freshwater is retained on the shelf, decreasing shelf salinity and increasing total shelf mass. The relationships between these fields are stronger in CM4 (Figures 11a and 11b) compared to ESM4 (Figures 11d and 11e), due to the stronger and more well-defined mean-state ASC.

The above results suggest that the strong ASC acceleration due to the meltwater perturbation in AntwaterStress would act to further limit open ocean and shelf exchange, thus effectively trapping the meltwater on the shelf. Given the stronger mean-state ASC and stronger acceleration in CM4 in AntwaterStress, this trapping hypothesis suggests that CM4 would retain more of the meltwater on the shelf compared to ESM4. To further examine this hypothesis, we examine time series of shelf salinity, total mass on the shelf, and ASC strength for ensemble members that start with similar mean-state ASC strengths of ∼10 Sv at 20°E (weaker period in CM4, stronger period in ESM4) and similar average shelf salinities (∼34.5 psu; Figures 11c and 11f). In this case, in ESM4, the shelf salinity drops slightly within the first ∼20 years and then plateaus for the rest of the simulation, while the ASC accelerates to ∼17 Sv and plateaus in the same time period (Figure 11f). On the other hand, in CM4, the shelf salinity steadily drops until about ∼35 years into the simulation, thus leading to a much fresher shelf (see Figures 6 and 7) before plateauing for the remainder of the simulation (Figure 11c). This period of rapid freshening corresponds to the same time period where the ASC accelerates from ∼10 to ∼35 Sv. For the same meltwater input, more mass is retained on the shelf in CM4 compared to ESM4 (red lines in Figures 11c and 11f).

21699291, 2022, 5, Downloaded from https://agupubs.onlinelibrary.wiley.com/doi/10.1029/2021JC017608 by University Of St Andrews University, Wiley Online Library on [08/11/2022]. See the Terms and Conditions (https://onlinelibrary.wiley.com/terms-and-conditions) on Wiley Online Library for rules of use; OA articles are governed by the applicable Creative Commons License

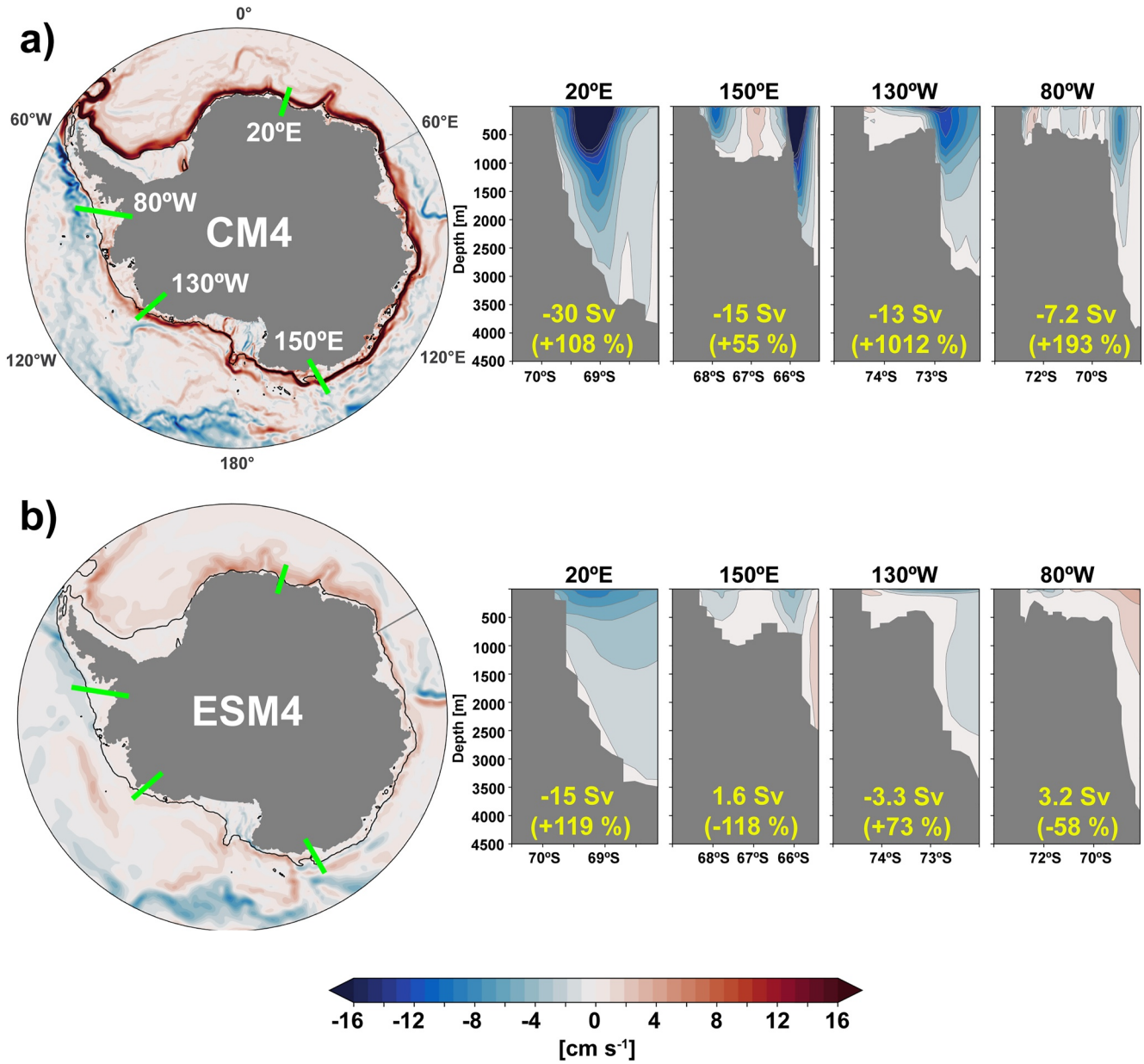

Figure 10. Ensemble-mean change in ocean speed (cm s^{-1}) depth-averaged over the upper 500 m and the ensemble-mean velocity (cm s^{-1}) at four transects along the Antarctic coast for the last 20 years of the (a) CM4 and (b) ESM4 AntwaterStress experiments. The transects and transports are the same regions and follow the same methods as described in the caption of Figure 9. The speed anomaly plots and the velocity sections share the same color bar. For the zonal velocity panels, red regions indicate eastward flow and blue regions indicate westward flow. For the speed anomalies, red indicates an increase in speed and blue indicates a decrease. The strength averaged over the last 20-year of the AntwaterStress experiment and the percent change relative to the piControl value are listed on the velocity speed panels. The 1,000 m isobath is contoured in each polar projection.

In CM4, a change in slope of the time series of the change in mass on the shelf coincides with the time period that the ASC accelerates to its maximum value.

4. Discussion

4.1. Limited Sensitivity of the Surface Layer in the Weddell Sea to Meltwater Forcing

A robust regionality was found when examining the sea ice and surface response in the subpolar SO in the AntwaterStress simulations across all ensemble members; a strong cooling of SAT and thickening of sea ice in the South

21699291, 2022, 5, Downloaded from https://agupubs.onlinelibrary.wiley.com/doi/10.1029/2021JC017608 by University Of St Andrews University, Wiley Online Library on [08/11/2022]. See the Terms and Conditions (https://onlinelibrary.wiley.com/terms-and-conditions) on Wiley Online Library for rules of use; OA articles are governed by the applicable Creative Commons License

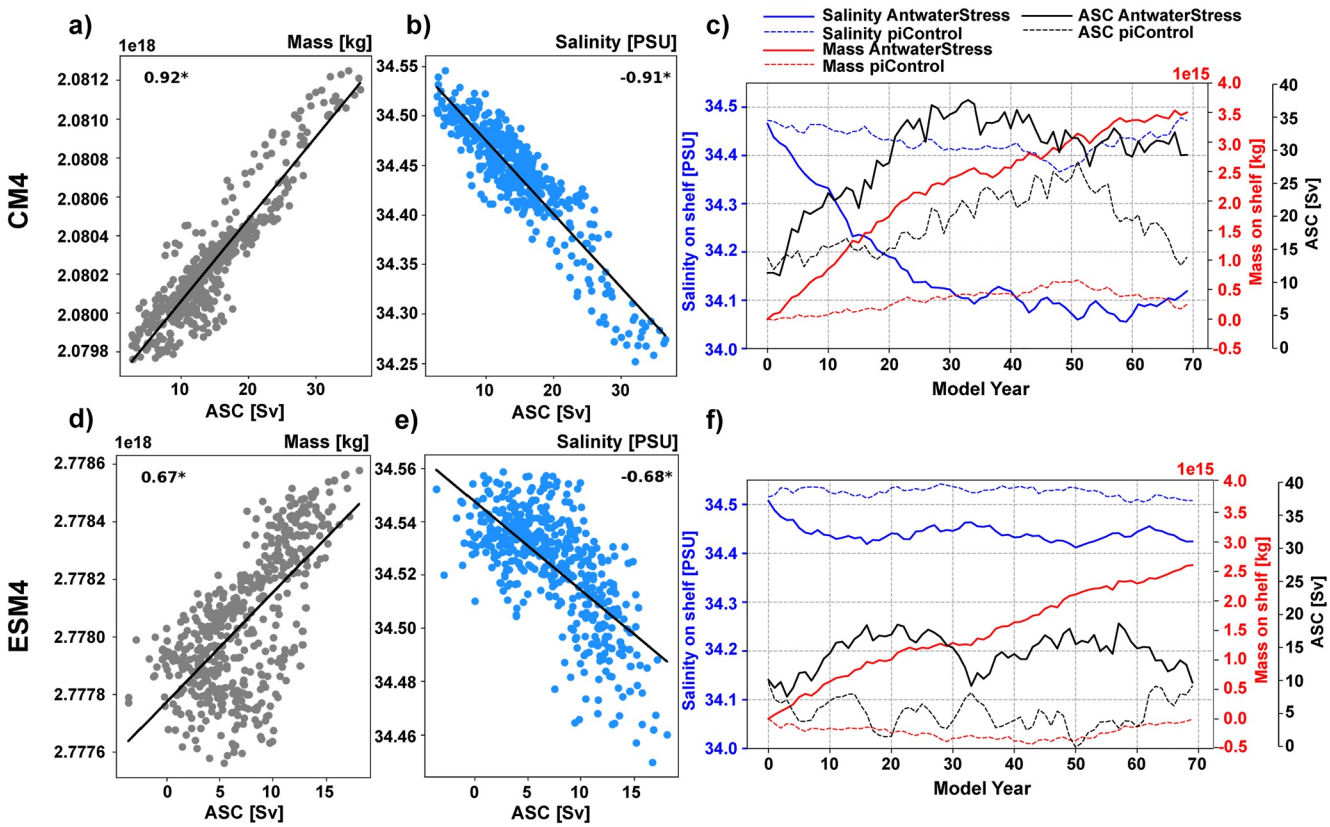

Figure 11. (a, b, d, e) Relationship between ASC strength and total mass and average salinity on the continental shelf over 500 years of each models' piControl integration (years 151–651 in CM4; years 101–600 in ESM4) with R^2 values shown in each panel. The shelf is defined as the region poleward of the 1,000 m isobath since this region tracks the Antarctic Slope Front (ASF) well, and thus represents the area poleward of the ASC. (c, f) Time series of average shelf salinity, ASC strength at 20°E (multiplied by −1 for positive values), and change in total mass on the shelf relative to year 1 for the first ensemble member for AntwaterStress. Change relative to year one is plotted for total mass on shelf since the mean-state mass on the shelf differs between the two models given their difference in total shelf area due to resolution. The first ensemble member is chosen to display since this represents a scenario where the models are starting from similar baseline states of shelf salinity and ASC strength. For comparison, we also plot the corresponding piControl time series for each field. An ensemble mean of these properties is not dynamically consistent with the relationships shown here given the varying initial states. The Pearson correlation coefficient (r) values for the AntwaterStress time series of ASC versus shelf salinity are −0.89 and −0.37 for the CM4 and ESM4 simulations, respectively and r values for the AntwaterStress time series of ASC versus shelf mass are 0.78 and 0.78, respectively. The correlation coefficients for all ensemble members are given in Table A2.

Pacific and a warming and thinning of sea ice in the Weddell Sea. This result suggests that the surface layer in the subpolar South Atlantic is sensitive to changes in the wind stress perturbations and yet not very sensitive to the imposed meltwater forcing. The dominance of the meltwater signal in the South Pacific is not surprising given that ∼75% of the total meltwater perturbation enters this region. The South Pacific is also a region where relatively flat isopycnals in the upper ocean and a lack of a dynamical barrier such as the ASC between the shelf and open ocean allows the freshwater to be more easily advected away from the shelf.

In the Pacific, the increased momentum from the enhanced and poleward shifted winds is not enough to overcome or compensate for the enhanced stratification from the surface freshening. Yet, the enhanced momentum from the wind stress dominates the response in the Weddell Sea. There are several reasons why this distinction results. One contributing factor is there is less direct meltwater input in the South Atlantic surface layer given that the largest observed mass loss from the AIS occurs in West Antarctica, concentrated along the WAP and from glaciers that flow into the Amundsen and Bellingshausen Seas (Paolo et al., 2015; Rignot et al., 2019; The IMBIE team, 2018). This regional variability in melt likely contributes to why regionality in the surface response has not been documented in studies that impose a spatially uniform meltwater distribution.

A significant fraction of the meltwater flows into the South Atlantic at midlatitudes as is clearly seen by the freshening and cooling signals in the surface and subsurface between 35° and 50°S (Figures 2, 3, and 6). This is a result of the advection of the meltwater by the eastward flowing ACC; however, the bathymetry of the Scotia Arc forces

21699291, 2022, 5, Downloaded from https://agupubs.onlinelibrary.wiley.com/doi/10.1029/2021JC017608 by University Of St Andrews University, Wiley Online Library on [08/11/2022]. See the Terms and Conditions (https://onlinelibrary.wiley.com/terms-and-conditions) on Wiley Online Library for rules of use; OA articles are governed by the applicable Creative Commons License

the ACC northward into the Argentine basin, away from the Weddell. Thus, the observed spatial distribution of meltwater and the regional bathymetry appears to somewhat "protect" the open ocean in the Weddell Sea from the strong freshening that emanates from the Pacific.

The westward flowing ASC and ACoC provide a pathway for the circumpolar advection of meltwater from West Antarctica to the Weddell. This transport is evidenced by fresh anomalies found along the shelf and continental slope and enhanced subsurface warming just offshore in the Weddell (Figures 6 and 20°E panels in Figures 7 and 8). The subsurface warming is associated with a reduction in the upward vertical mixing of heat due to the enhanced stratification, a robust result documented in other previous meltwater studies (Bronselaer et al., 2018; Sadai et al., 2020). The ASC and boundary currents constrain the largest anomalies to the boundaries of the Weddell Gyre, particularly in CM4. In ESM4, the pattern of the Weddell Sea subsurface response is more spatially homogeneous in the Antwater experiments and a more complex pattern arises in AntwaterStress. The causes of these differences between the models are discussed in the subsequent sections.

4.2. Mechanism of Wind-Driven Surface Warming in the Weddell Sea

We first discuss the mechanisms of warming in the Stress simulations, as these same mechanisms apply to the warming in the Weddell Sea in AntwaterStress. Considering the Stress simulation by itself, our results agree with previous studies where strengthened and poleward shifted westerlies enhance Ekman pumping and drive more relatively warm and saline CDW to the surface (Bronselaer et al., 2020; Spence et al., 2014). Additionally, in both models, the coastal easterlies weaken as the westerlies shift poleward, reducing the Ekman pumping along the shelf break which shoals the isopycnals and allows more relatively warm and saline CDW to access the shelf. In the Stress simulations, the enhanced upwelling of relatively warm subsurface water warms the upper ocean and limits sea ice growth, causing thinning and a reduction in SIE. A simultaneous reduction in surface albedo occurs, contributing to further SAT warming.

The enhanced and poleward shifted westerlies may also influence sea ice properties in the subpolar SO through a deepening of the summertime mixed layer. We did not diagnose this change in our analysis, however, previous studies suggest these mechanisms could lead to increased subsurface heat storage that may reemerge to the surface layer as the mixed layer deepens in the subsequent autumn and winter (Doddridge et al., 2021). The diminished state of sea ice in the Stress simulations allows for localized increases in surface heat fluxes from the ocean to the atmosphere, while also preconditioning the subpolar SO for the formation of large open ocean polynyas that release a large amount of heat to the overlying atmosphere.

Model-dependent results are found in the Stress experiments. The warming response of SAT and SST to the Stress perturbation in ESM4 is double that in CM4. This behavior is a result of the warmer subsurface SO in ESM4 in its piControl state (Figures 6 and 8 and Dunne, Horowitz, et al., 2020). This warmer subsurface is partly linked to an overly shallow and warm NADW in ESM4 (Dunne, Horowitz, et al., 2020). The subsurface ocean is particularly warm in ESM4 in the South Atlantic and Indian oceans adjacent to the shelf. In the Stress experiments, this anomalously warm water is upwelled, triggering large polynyas in the Weddell Sea, which leads to a complete loss of wintertime sea ice in this sector for several winters, sustained deep convection, and associated strong warming that is not found in CM4.

The same mechanisms discussed above govern the response found in the AntwaterStress experiments; however, the wind stress perturbation only significantly influences the surface response in the Weddell Sea, with the surface cooling induced via increased stratification from the meltwater dominating elsewhere. The warming in the Weddell Sea in the AntwaterStress experiments is more pronounced in CM4 relative to ESM4, despite ESM4 having a larger warming in the Stress simulations as noted above. These differences suggest that the meltwater is having a larger influence on stratification in the Weddell Sea in ESM4 relative to CM4. The time series of maximum mixed layer depths in the Weddell Sea supports this hypothesis. Namely, all CM4 AntwaterStress ensemble members show deep convective events (which warm SATs) occurring in the open ocean, while open ocean deep convection ceases in ESM4. We discuss why the meltwater exerts a greater influence on open ocean properties in ESM4 in the next section.

21699291, 2022, 5, Downloaded from https://agupubs.onlinelibrary.wiley.com/doi/10.1029/2021JC017608 by University Of St Andrews University, Wiley Online Library on [08/11/2022]. See the Terms and Conditions (https://onlinelibrary.wiley.com/terms-and-conditions) on Wiley Online Library for rules of use; OA articles are governed by the applicable Creative Commons License

4.3. Role of the ASC in Determining the Antarctic Shelf Response

The meltwater perturbation dominates the Antarctic shelf response in the AntwaterStress simulations. Despite being forced with the same spatial distribution of meltwater input, CM4 and ESM4 yield very different patterns of salinity anomalies along the shelf. Opposite responses are found at depth on the West Antarctic shelf, with strong freshening and cooling in CM4 versus strong warming and salinification in ESM4 (Figures 6–8). The disagreement between the models in this region highlights a large uncertainty with respect to how ice shelves in West Antarctica will respond to increased meltwater, with this region being where most of the observed Antarctic ice shelf melting occurs (Paolo et al., 2015; Shepherd et al., 2004; The IMBIE team, 2018). The strong cooling and freshening at depth on the West Antarctic shelf in CM4 agree with previous results using an eddy-permitting ocean-sea-ice model at 0.1° horizontal grid spacing forced with meltwater perturbations under a piControl state (Moorman et al., 2020). The strong subsurface warming and increased salinity in this same region in ESM4 are consistent with results from similar experiments utilizing coarse models at ∼1° horizontal grid spacing (Bronselaer et al., 2018; Fogwill et al., 2015; Golledge et al., 2019; Menviel et al., 2010). We propose that these differences are attributable to the different mean-state representations and responses of the ASC to the meltwater perturbations. The differences and mechanisms are discussed below and summarized in Figure 12.

Shelf freshening in CM4 accelerates the flow on and adjacent to the shelf, advecting the meltwater away from the source regions and homogenizing the salinity patterns along the shelf, leading to deep circumpolar fresh anomalies. A strong feedback is established where (a) shelf freshening increases the lateral density gradient between the shelf and open ocean, (b) the enhanced cross-shelf density gradient accelerates the ASC, (c) a stronger ASC and ACoC homogenize the shelf salinity, (d) the strong ASC acts as a dynamical barrier limiting exchange between the shelf and open ocean, which (e) leads to further shelf freshening. This process occurs until the ASC plateaus at a maximum strength of ∼35 Sv at 20°E (Figure A4; maximum value depends on region).

In CM4, the West Antarctic shelf region transitions from a region characterized by relatively flat or upward sloping isopycnals that outcrop onto the shelf, allowing warm and saline CDW to flood the shelf, to a region characterized by steep downward sloping isopycnals that limit CDW shelf exchange. In the piControl simulations, the regime adjacent to the continental shelf along the WAP is dominated by eastward flow associated with the ACC. In the CM4 AntwaterStress experiment, the eastward flow is replaced by westward flow between the shelf and open ocean, establishing an ASC where there once was none. This change isolates the West Antarctic shelf from heat fluxes associated with offshore CDW, leading to very strong cooling. Additionally, the establishment and strengthening of the westward flow along the slope redirect waters from the Weddell Sea, through the Drake Passage, and onto the West Antarctic shelf. While the subsurface signal is dominated by the meltwater-driven cooling, the weakened coastal easterlies in the AntwaterStress experiment do compensate for some of this cooling, shoaling the isopycnals and reducing the subsurface cooling anomaly relative to the Antwater simulation. The isopycnal slopes shown in the shelf cross-section along the WAP for the AntwaterStress experiment in CM4 (Figures 7 and 8) indicate that this region is not completely isolated from the open ocean. These results and mechanisms described above are generally consistent with those from Moorman et al. (2020) and agree with their suggestion that there may be a negative feedback to increased meltwater that *limits* future warming along the West Antarctic shelf. Our results suggest that the projected changes in the wind stress field can act to limit the magnitude of this subsurface cooling and still allow for limited connection between the shelf and open ocean, leading to an incomplete isolation. Results from a 1% per year CO_2 simulation using an eddy-permitting fully coupled model also support an acceleration of the ASC and shelf isolation mechanism in response to shelf freshening, however of a much lesser magnitude as that simulation only included freshening due to an enhanced hydrological cycle (Goddard et al., 2017).

Similar to Moorman et al. (2020), the strong cooling (and decrease in ocean age) along the West Antarctic shelf in CM4 coincides with Weddell shelf water forming at lighter densities (not shown). Moorman et al. (2020) posit that the cooling and isolation mechanism along the West Antarctic shelf is dependent on the meltwater-driven reduction in buoyancy of the waters on the Weddell shelf and their diversion eastward around the WAP as opposed to cascading down the continental slope and contributing to overturning as AABW. Our current analysis cannot explicitly disentangle the cause of the sharp steepening of the isopycnals and parallel establishment of an ASC along the West Antarctic continental slope, that is, whether this is a direct result of the large amount of meltwater entering the coast in this region which enhances the local cross-shelf density gradient or whether this is a result

21699291, 2022, 5, Downloaded from https://agupubs.onlinelibrary.wiley.com/doi/10.1029/2021JC017608 by University Of St Andrews University, Wiley Online Library on [08/11/2022]. See the Terms and Conditions (https://onlinelibrary.wiley.com/terms-and-conditions) on Wiley Online Library for rules of use; OA articles are governed by the applicable Creative Commons License

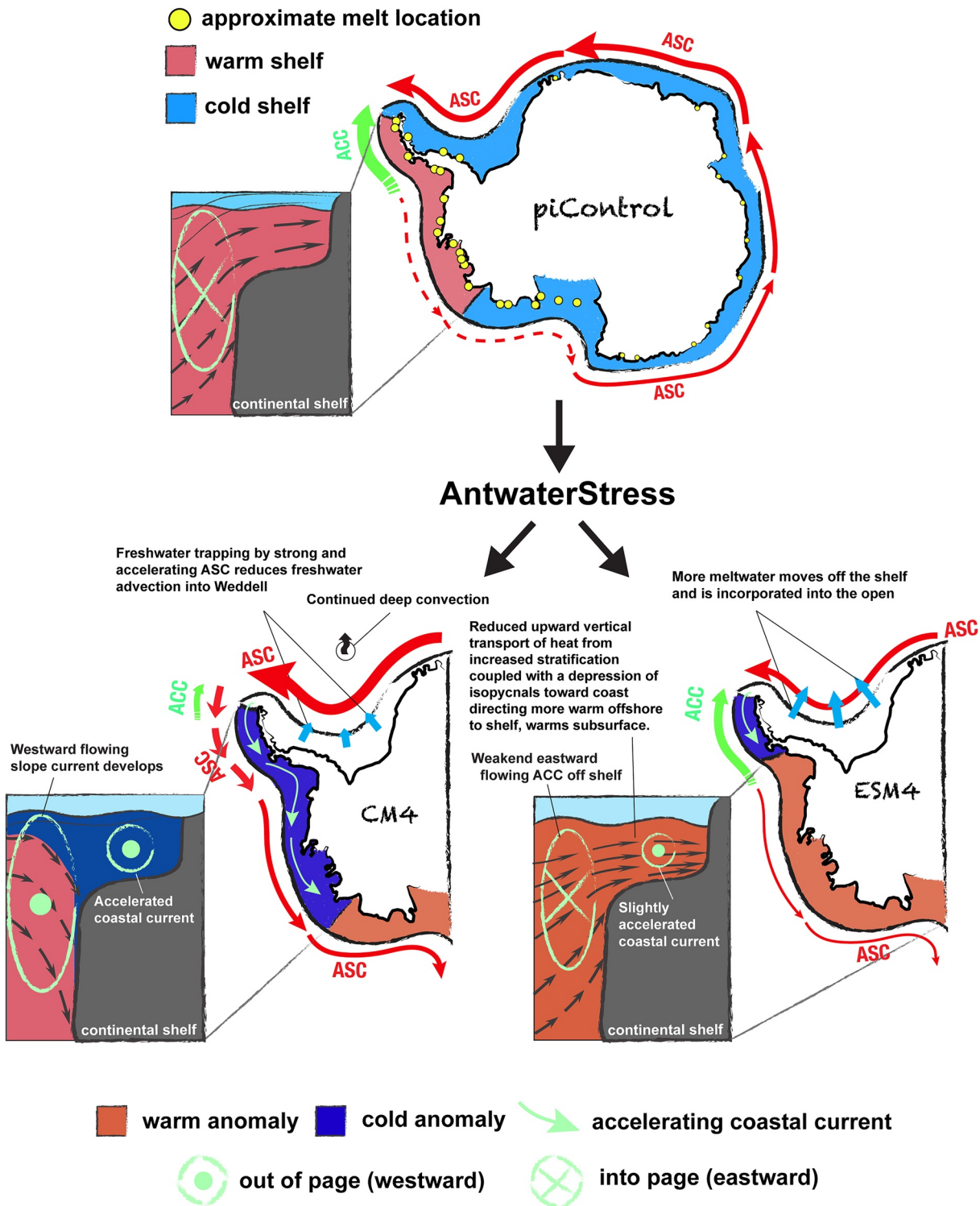

Figure 12. Schematic representation of the key processes that explain the differing response to the AntwaterStress perturbation along the Antarctic shelf in CM4 and ESM4.

of the cold and fresh water rerouting from the Weddell shelf into this region and in turn causing a steeping of the cross-shelf density gradient. It is likely a combination of these two mechanisms acting on the ASF and thus impacting the ASC and cross-slope exchange.

21699291, 2022, 5, Downloaded from https://agupubs.onlinelibrary.wiley.com/doi/10.1029/2021JC017608 by University Of St Andrews University, Wiley Online Library on [08/11/2022]. See the Terms and Conditions (https://onlinelibrary.wiley.com/terms-and-conditions) on Wiley Online Library for rules of use; OA articles are governed by the applicable Creative Commons License

In ESM4, the weaker and more diffuse mean-state ASC leads to less freshwater retention on the shelf compared to CM4. This difference is indicated by the lack of strong and homogenous fresh anomalies and lower values of total mass on the shelf throughout the simulation despite the same freshwater forcing. The ASC does accelerate in ESM4 suggesting a similar but much weaker feedback to the shelf freshening relative to CM4. As in Lockwood et al. (2021), without a strong dynamical barrier from the ASC, freshwater can more easily escape to the open ocean, impacting sea ice properties and leading to the cessation of deep convective events despite the enhanced and poleward shifted Southern Hemisphere westerlies in AntwaterStress. Unlike CM4, the eastward flow adjacent to the West Antarctic shelf weakens in ESM4 but is not replaced by a westward flowing ASC. Thus, there is no shelf isolation mechanism in ESM4. Along the tip of the WAP there is evidence that accelerating coastal currents are transporting some recently ventilated Weddell Sea water onto the West Antarctic shelf. Increased stratification driven by surface freshening and enhanced onshore transport of CDW appear to be the primary mechanism governing the response along the West Antarctic shelf. The subsurface salinity and temperature anomalies are slightly larger in these regions in the AntwaterStress experiment relative to Antwater, suggesting the wind-driven shoaling of isopycnals does have a noticeable influence in controlling the magnitude of subsurface warming in ESM4. The ESM4 results are generally consistent with that of Bronselaer et al. (2018), who imposed a uniform meltwater flux at the surface along the Antarctic coast in an Earth system model with a 1° ocean grid spacing and found enhanced subsurface warming along the shelf. The authors proposed a mechanism by which the depression of isopycnals near the Antarctic coast driven by surface freshening can cause the transport of relatively warm and saline CDW toward the shelf rather than toward the ocean surface. This mechanism, in addition to subsurface warming from enhanced stratification, would suggest an establishment of a positive feedback where the warmer subsurface waters on the shelf would enhance basal melting of the adjacent ice shelves.

The strength and structure of the ASC are a primary contributor to the different responses found between CM4 and ESM4 along the Antarctic shelf. In CM4, a strong ASC is simulated, and a strong isolation mechanism develops in response to the meltwater perturbations in which the shelf becomes isolated from the open ocean, leading to a trapping of the meltwater on the shelf. In contrast, this behavior is not present in ESM4 which has a weaker and less defined ASC. Some factors that contribute to the differing ASC representations include differing horizontal grid resolutions, with finer horizontal resolution in CM4 allowing the properties across the ASF to be better resolved. The finer resolution of the continental slope bathymetry in CM4 improves its ability to resolve a well-defined ASC structure since the conservation of planetary geostrophic potential vorticity (in a homogeneous fluid layer) requires the ASC to closely follow contours of f/h (Pedlosky, 1987; Thompson et al., 2018). Here, f is the Coriolis parameter and h is the water column depth. Thus, the improved representation of the horizontal topographic gradient, or slope steepness, in CM4 acts to stabilize the structure and steer the ASC. Resolving topographic features along the shelf-slope interface can also act as barriers to isopycnals outcropping onto the shelf and thus influence shelf properties and gradients across the ASF. However, the fact that the horizontal resolution in CM4 is insufficient for fully resolving mesoscale eddies at the latitudes of the ASC and no mesoscale eddy parameterization is employed is important to consider. Without this mechanism to oppose the steepening of isopycnals along the shelf break in CM4, the steepening of the ASF and parallel acceleration of the ASC in response to the meltwater may be overly strong (see also Goddard et al., 2017; Lockwood et al., 2021). This issue warrants further exploration.

We have focused our analysis and discussion here on the influence of the ASC, however, there is also a growing body of literature that DSW formation and its descent down the continental slope is an important factor that mediates cross-slope exchange (Moorman et al., 2020; Morrison et al., 2020; Snow et al., 2016). Thus, a model's ability to represent DSW production and overflows is likely to impact the representation of Antarctic shelf properties and their changes in response to wind and meltwater perturbations. Both CM4 and ESM4 form AABW through both open-ocean polynyas and DSW formation. How this impacts their response to the wind and meltwater forcings warrants a further detailed study. Formation and export of DSW and the ASC are intimately tied together, with DSW formation and its ability to draw heat onshore impacting the strength and velocity structure of the ASC, and the ASC acting as a dynamical barrier that directly modulates the properties of the shelf waters from which DSW are sourced. Due to this complexity, a wealth of further work is needed to fully understand the dynamics that dominate the thermal response on the Antarctic shelf and the role that both the ASC and DSW changes play.

21699291, 2022, 5, Downloaded from https://agupubs.onlinelibrary.wiley.com/doi/10.1029/2021JC017608 by University Of St Andrews University, Wiley Online Library on [08/11/2022]. See the Terms and Conditions (https://onlinelibrary.wiley.com/terms-and-conditions) on Wiley Online Library for rules of use; OA articles are governed by the applicable Creative Commons License

5. Summary and Conclusions

Using two similar fully coupled models with different mean-state representations of the ASC, we investigated the transient response of the SO to increased Antarctic meltwater, projected wind stress change, and the two forcings combined. In both models, the meltwater and wind stress perturbations have significant—but opposite—impacts on surface properties globally and in the SO. When imposed simultaneously, an asymmetric surface response is found with cooling and sea ice thickening in all regions of the subpolar SO apart from the Weddell Sea, where warming and sea ice thinning occur. This regional warming and slight compensation by the wind stress perturbation reduces the amount of global and regional cooling relative to the response from the meltwater alone. The larger surface temperature response to the meltwater perturbation, more homogenous sea ice thickening, and weaker surface warming in the combined forcing experiment in ESM4 suggested that the meltwater exerted a greater influence on the open ocean compared to CM4.

By acting as a dynamical control on the advection of meltwater away from the Antarctic shelf, the mean-state strength, structure, and acceleration of the ASC contribute to the strikingly different Antarctic shelf response in the two models. The response to the perturbations along the West Antarctic shelf reveals a *"tale of two possible melt-rate feedbacks."* Although no ice shelf-ocean feedback processes are represented in these models since the melt rate is prescribed, the strong subsurface shelf cooling in CM4 would act as a mechanism to limit future ice sheet melting, while the strong subsurface shelf warming in ESM4 would act to accelerate future melt. In the case of CM4, a strong, well-defined, and accelerating ASC traps fresh anomalies tightly to the shelf and a westward current develops along the West Antarctic shelf where it was previously absent. This process isolates the West Antarctic shelf regime from warm CDW intrusions, causing a strong subsurface cooling. Isopycnal shoaling associated with wind stress forcing act as a control on the magnitude of the subsurface cooling, aiding to maintain a connection between the shelf and open ocean. In a coupled ice-ocean system, as subsurface temperatures cool and additional basal melting becomes limited, warm CDW intrusions onto the shelf may recover. The constant 0.1 Sv forcing is not temperature-dependent and cannot represent this feedback. The plausibility and timing over which these feedback mechanisms may operate to control CDW shelf intrusions need to be explored using a modified temperature-dependent meltwater flux, or better yet, a fully coupled interactive ice sheet model. In ESM4, the mean-state ASC is weak and diffuse, more meltwater escapes from the shelf into the open ocean, and the ASC does not experience a strong acceleration. Enhanced stratification from surface freshening and increased shoreward transport of CDW leads to strong subsurface warming along the West Antarctic shelf in ESM4.

Although these experiments were performed under a preindustrial control state, the strong model disagreement on the thermal response in West Antarctica raises a high degree of uncertainty in the projected response in a region where most of the ice shelf melt is occurring. Our results highlight that models with sufficient resolution to resolve the ASC responds differently to meltwater perturbations compared to coarse resolution models that have a less well-defined ASC or none at all. Given the influence of the ASC on shelf properties, it is crucial that the models used to derive fields to force ice-sheet models or are coupled to an interactive ice sheet model are able to resolve the ASC in order to understand present-day changes along the Antarctic shelf and derive more robust future projections. The presence (ESM4) or lack of (CM4) parameterized eddy effects may contribute to the efficiency of which the ASC acts as a dynamical barrier between the shelf and open ocean, however, our present experimental design cannot quantify this effect.

A robust assessment of the ASC and ASF mean-state and temporal variability in models requires sustained observations of velocity, temperature, and salinity on the Antarctic shelf and across the continental slope. Existing observations of these properties in conjunction with one another are sparse, limited to short windows of time (2 years or less), and are at differing locations (Bindoff et al., 2000; Costa et al., 2008; Heywood et al., 2012, 2014; Meijers et al., 2010; Peña-Molino et al., 2016). Owing to its remote location, difficulties with autonomous observations along steep slopes and in regions with shallow bathymetry, and the fact that the ASC is under sea ice for large portions of the year, achieving sustained observations is challenging. However, the results presented here, particularly the influence of the ASC on the thermal properties of waters that interact with the AIS, highlight the need for new and continued observations to understand the dynamics of and consequences of change in this climatically important region.

21699291, 2022, 5, Downloaded from https://agupubs.onlinelibrary.wiley.com/doi/10.1029/2021JC017608 by University Of St Andrews University, Wiley Online Library on [08/11/2022]. See the Terms and Conditions (https://onlinelibrary.wiley.com/terms-and-conditions) on Wiley Online Library for rules of use; OA articles are governed by the applicable Creative Commons License

Moving forward, these simulations will be performed under a scenario accounting for increases in atmospheric CO_2, as ocean warming also exerts an influence on ocean stratification and imposing the perturbations in a warming climate may yield different results. Following Moorman et al. (2020), we imposed the meltwater fluxes in regions of observed ice shelf melting rather than a spatially uniform flux. However, all freshwater enters at the surface and directly on the shelf, while in nature, freshwater discharge from the AIS occurs through basal melting at the grounding lines in the subsurface ocean and through iceberg calving (a mechanism that can deliver fresh water away from the shelf) (Rignot et al., 2013; Deeporter et al., 2013; Stern et al., 2016; Mackie et al., 2020). Additionally, we did not include any temporal variability or vertical structure in the meltwater perturbations. However, meltwater discharge from iceberg calving and basal melting varies seasonally (Schlosser et al., 2019) and the interplay between the timing of freshwater release and the state of local ocean stratification likely impacts the fate of the meltwater and its impact on ocean properties. Additional simulations will explore the dependency of the response on the spatial distribution and partitioning of the meltwater fluxes.

The uncertainty of whether AIS meltwater will drive a subsurface cooling response or a subsurface warming response along the shelf translates into a large uncertainty in future melt-rate and associated global and regional sea level rise. There is a wide range in the ability of models contributed to the Coupled Model Intercomparison Project (CMIP) to represent properties in the subpolar SO and along the continental shelf (Beadling et al., 2019, 2020; Heuzé et al., 2021; Meijers, 2014; Purich & England, 2021; Sallée et al., 2013). The uncertainty of performing these simulations on models with various mean-state representations of SO circulation, density structures, and dense water formation mechanisms (i.e., resolving DSW overflows vs. open ocean polynyas) needs to be explored. If the subsurface cooling and negative feedback mechanism proves to be robust, this would provide a strong argument for the use of high-resolution model output for offline forcing of ice-sheet models or coupling with interactive ice-sheet models to derive better estimates of sea level rise and projections of other global metrics due to AIS mass loss.

Appendix A: Additional Details on Experimental Design and Analysis of Perturbation Experiments

This Appendix contains additional details regarding experimental design including an outline the perturbations considered in this study (Table A1) and the time evolution of the mean-state subsurface heat reservoir in the Ross Sea in the piControl simulations (Figure A1), which was used to inform the initialization point of ensemble members. Additional analysis is also shown addressing the linearity of the surface response to the wind and meltwater forcing (Figure A2), ideal age anomalies along the Antarctic shelf in the AntwaterStress experiments (Figure A3), the time evolution of the ASC response to the perturbations (Figure A4), and the temporal correlations between shelf properties and the ASC (Table A2) throughout the experiments.

21699291, 2022, 5, Downloaded from https://agupubs.onlinelibrary.wiley.com/doi/10.1029/2021JC017608 by University Of St Andrews University, Wiley Online Library on [08/11/2022]. See the Terms and Conditions (https://onlinelibrary.wiley.com/terms-and-conditions) on Wiley Online Library for rules of use; OA articles are governed by the applicable Creative Commons License

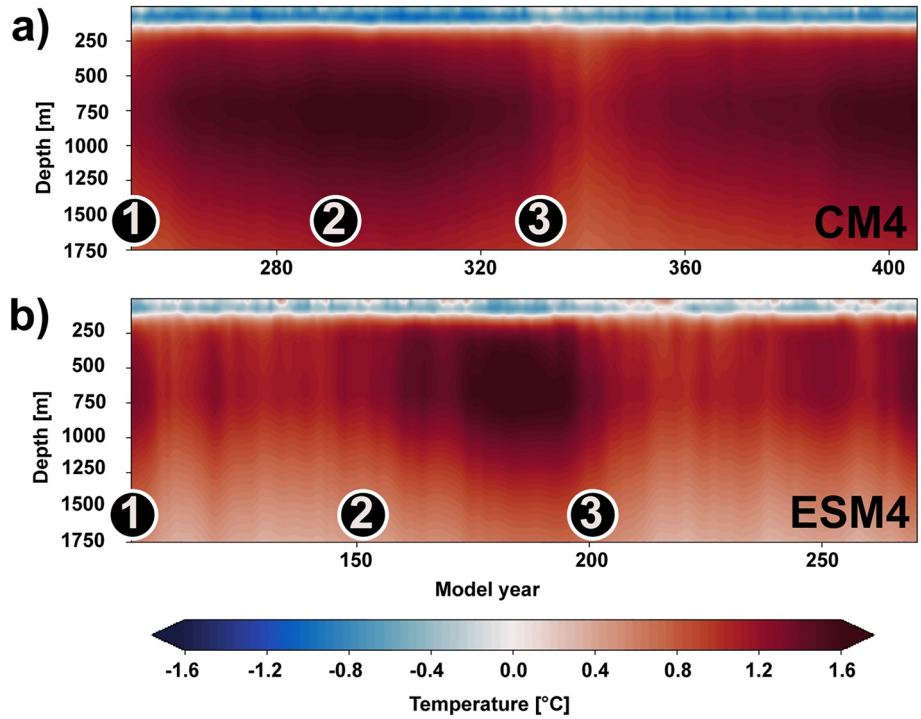

Figure A1. Hovmöller plot of annual-mean Ross Sea (averaged over 160° −230°E and 60° −90°S) ocean temperature in the piControl simulations for (a) CM4 and (b) ESM4. The initialization point for each ensemble member (1–3) is shown as the labeled black circles on each panel.

21699291, 2022, 5, Downloaded from https://agupubs.onlinelibrary.wiley.com/doi/10.1029/2021JC017608 by University Of St Andrews University, Wiley Online Library on [08/11/2022]. See the Terms and Conditions (https://onlinelibrary.wiley.com/terms-and-conditions) on Wiley Online Library for rules of use; OA articles are governed by the applicable Creative Commons License

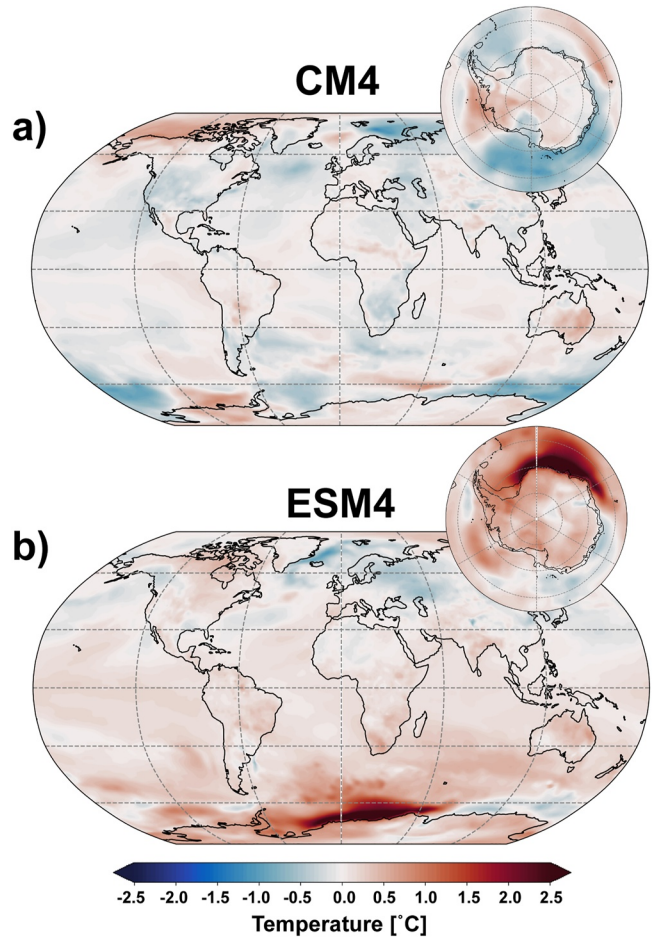

Figure A2. Ensemble-mean annual-mean surface air temperature (SAT; °C) difference between the summation of the anomalies of the individual Antwater and Stress experiments (Antwater + Stress) and the AntwaterStress experiment for (a) CM4 and (b) ESM4. This was done to investigate the linearity of the AntwaterStress response to the response from the single forcing experiments (Antwater and Stress). Red (blue) values indicate regions where the summation of the Antwater and Stress experiments produce SAT anomalies warmer (cooler) than those simulated in the AntwaterStress experiment. The 1000 m isobath is contoured in each polar projection.

21699291, 2022, 5, Downloaded from https://agupubs.onlinelibrary.wiley.com/doi/10.1029/2021JC017608 by University Of St Andrews University, Wiley Online Library on [08/11/2022]. See the Terms and Conditions (https://onlinelibrary.wiley.com/terms-and-conditions) on Wiley Online Library for rules of use; OA articles are governed by the applicable Creative Commons License

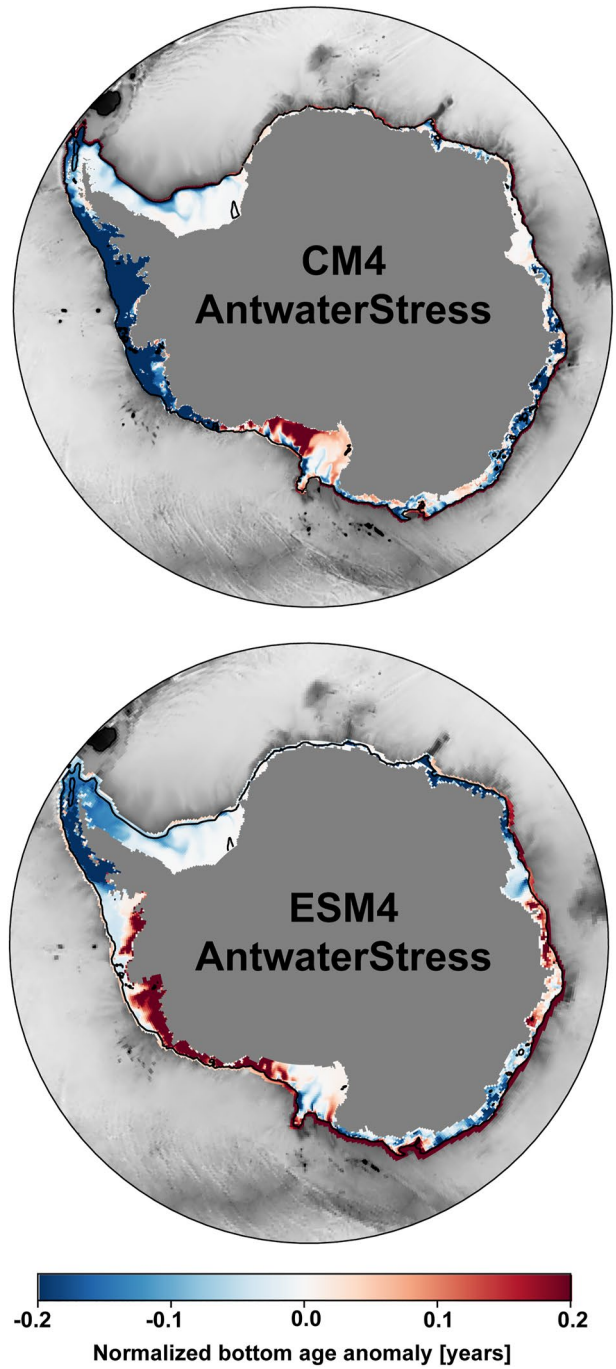

Figure A3. Ensemble-mean bottom age anomaly (years since surface contact) along the Antarctic shelf for the last 20 years of the AntwaterStress experiment. To normalize, the age at each grid cell is divided by the temporally varying spatial mean bottom age over the Southern Ocean. The 1,000 m isobath is contoured and the seafloor is shaded in gray.

21699291, 2022, 5, Downloaded from https://agupubs.onlinelibrary.wiley.com/doi/10.1029/2021JC017608 by University Of St Andrews University, Wiley Online Library on [08/11/2022]. See the Terms and Conditions (https://onlinelibrary.wiley.com/terms-and-conditions) on Wiley Online Library for rules of use; OA articles are governed by the applicable Creative Commons License

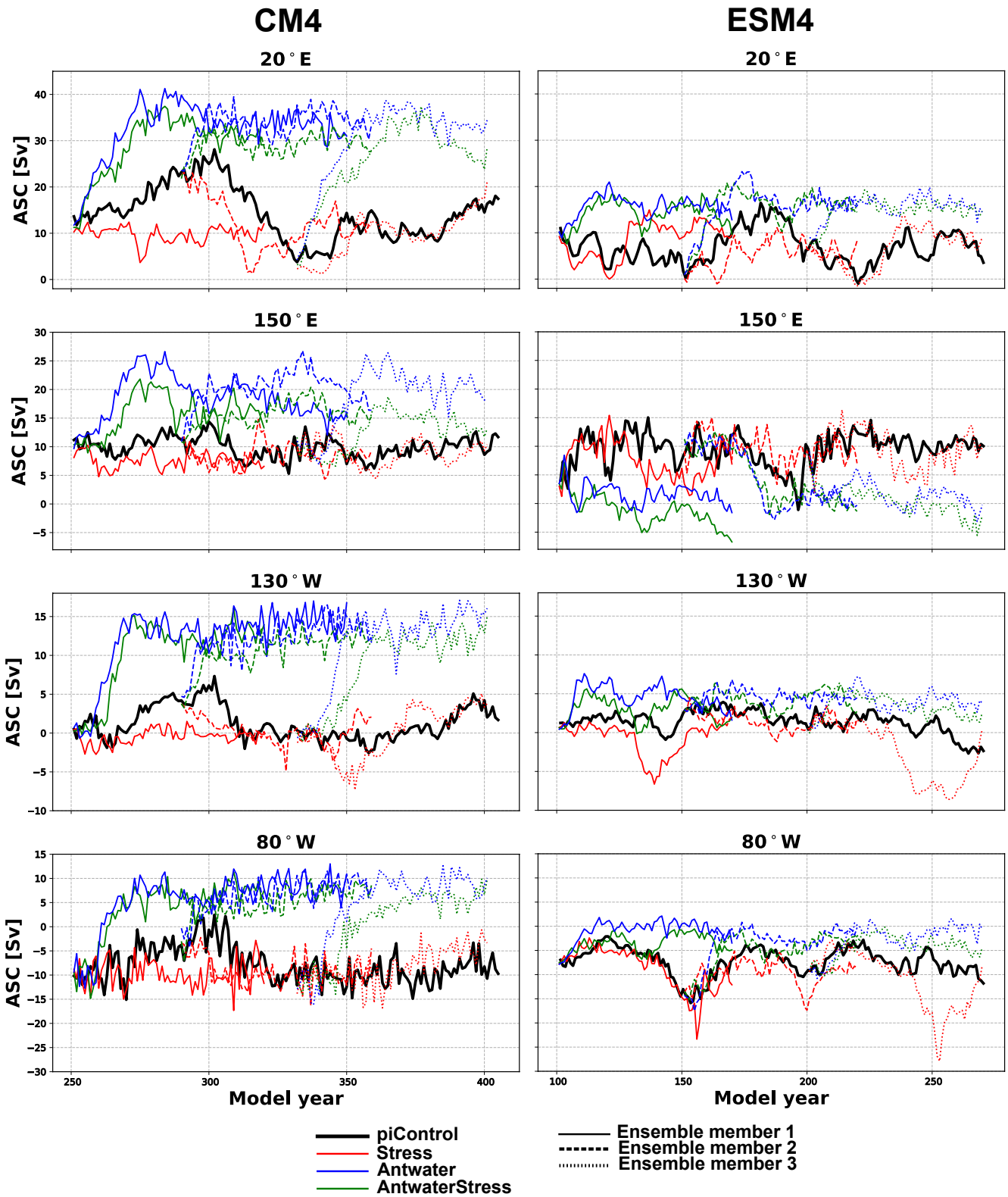

Figure A4. Strength of the Antarctic Slope Current (ASC; Sv) at the four locations around the Antarctic coast shown in Figure 9 for the entire piControl period that overlaps with each ensemble member, and the three different ensemble members that branch from the piControl integration for each perturbation experiment. The ASC transport has been multiplied by −1 here to get a net positive transport. In this case, positive values indicate net westward flow and negative indicated eastward flow.

21699291, 2022, 5, Downloaded from https://agupubs.onlinelibrary.wiley.com/doi/10.1029/2021JC017608 by University Of St Andrews University, Wiley Online Library on [08/11/2022]. See the Terms and Conditions (https://onlinelibrary.wiley.com/terms-and-conditions) on Wiley Online Library for rules of use; OA articles are governed by the applicable Creative Commons License

Table A1
Experiments Performed in This Study

Stress	Monthly FAFMIP zonal and meridional momentum flux perturbations applied to the surface wind stress fields. The momentum fluxes correspond to changes expected to occur at the time of CO_2 doubling from preindustrial control values (~middle of the 21st century under RCP8.5 or SSP5-8.5 scenarios).
Antwater	Time-uniform total of 0.1 Sv applied at the surface within a 1° latitude from the Antarctic coast in regions of observed melting following Paolo et al. (2015) and The IMBIE team (2018). Freshwater is assumed to be at SST. Contribution of freshwater flux from each grid cell is weighted based on observed rates of melt. The 0.1 Sv corresponds to the total flux expected near mid-century under RCP8.5 determined from dynamic ice-sheet model simulations (DeConto & Pollard, 2016).
AntwaterStress	Perturbations from Stress and Antwater applied simultaneously.

Note. Spatial patterns of the wind stress and meltwater perturbations are shown in Figure 1.

Table A2
Pearson Correlation Coefficients (r) for Relationships Between Antarctic Slope Current (ASC) Assessed at 20°E and Total Mass on the Shelf and Average Shelf Salinity for the Antwater and AntwaterStress Ensemble Members

	CM4 (*r*)	ESM4 (*r*)
Antwater 1		
ASC versus shelf salinity	−0.94	−0.73
ASC versus shelf mass	0.81	0.81
Shelf salinity versus shelf mass	−0.93	−0.45
Antwater 2		
ASC versus shelf salinity	−0.62	−0.77
ASC versus shelf mass	0.48	0.60
Shelf salinity versus shelf mass	−0.88	−0.11*
Antwater 3		
ASC versus shelf salinity	−0.96	−0.73
ASC versus shelf mass	0.87	0.59
Shelf salinity versus shelf mass	−0.95	−0.39
AntwaterStress 1		
ASC versus shelf salinity	−0.89	−0.37
ASC versus shelf mass	0.78	0.78
Shelf salinity versus shelf mass	−0.96	−0.45
AntwaterStress 2		
ASC versus shelf salinity	−0.41	−0.91
ASC versus shelf mass	0.31	0.52
Shelf salinity versus shelf mass	−0.92	−0.43
AntwaterStress 3		
ASC versus shelf salinity	−0.89	−0.76
ASC versus shelf mass	0.82	0.49
Shelf salinity versus shelf mass	−0.98	−0.23

Note. The shelf is defined as the region poleward of the 1,000 m isobath. The correlations are computed using the entire 70-year time period of the simulation. Values that are not statistically significant at the 95% confidence level are marked with an asterisk (*).

21699291, 2022, 5, Downloaded from https://agupubs.onlinelibrary.wiley.com/doi/10.1029/2021JC017608 by University Of St Andrews University, Wiley Online Library on [08/11/2022]. See the Terms and Conditions (https://onlinelibrary.wiley.com/terms-and-conditions) on Wiley Online Library for rules of use; OA articles are governed by the applicable Creative Commons License

Data Availability Statement

The forcing fields that were used in these experiments as well as the code to produce the figures can be found at (https://github.com/becki-beadling/Beadling_et_al_2022_JGROceans). All model output is available on request and is in the process of being made publicly available on the Earth System Grid Federation archive (https://esgf-node.llnl.gov/projects/cmip6/) as part of FAFMIP. The GFDL MOM6 code is openly available at https://github.com/NOAA-GFDL/MOM6.

Acknowledgments
This work was funded by NSF's Southern Ocean Carbon and Climate Observations and Modeling (SOCCOM) Project under NSF Award PLR-1425989, with additional support from NOAA and NASA. Logistical support for SOCCOM in the Antarctic was provided by the U.S. NSF through the U.S. Antarctic Program. This work was also supported by the U.S. DOE Subcontract no. B640108 under Prime Contract no. DE-AC52-07NA27344. RLB was additionally supported by the NOAA Climate and Global Change Postdoctoral Fellowship Award. The authors thank the FAFMIP team for production of the wind stress perturbation fields. The authors are thankful to the developers of the xarray (http://xarray.pydata.org/) and xgcm (https://xgcm.readthedocs.io/en/latest/) packages. The authors thank John Dunne and Robert Hallberg at NOAA's Geophysical Fluid Dynamics Laboratory, Ruth Moorman at California Institute of Technology for sharing code to investigate cross-isobath transports, Matthew Mazloff at Scripps Institution of Oceanography for providing the Southern Ocean State Estimate (SOSE) output, and the editor and two anonymous reviewers for comments and suggestions that greatly improved the paper. Computational resources for the SOSE were provided by NSF XSEDE resource grant OCE130007. The computational resources that allowed for the analysis presented in this manuscript sit on the ancient homeland and traditional territory of the Lenape people. The authors pay respect to Lenape peoples past, present, and future and their continuing presence in the homeland and throughout the Lenape diaspora.

References

Adcroft, A., Anderson, W., Balaji, V., Blanton, C., Bushuk, M., Dufour, C. O., et al. (2019). The GFDL Global Ocean and Sea Ice Model OM4.0: Model description and simulation features. *Journal of Advances in Modeling Earth Systems*, *11*, 3167–3211. https://doi.org/10.1029/2019ms001726

Baines, P. G. (2009). A model for the structure of the Antarctic slope front. *Deep-Sea Research Part II: Topical Studies in Oceanography*, *56*, 859–873.

Beadling, R. L., Russell, J. L., Stouffer, R. J., Goodman, P. J., & Mazloff, M. (2019). Assessing the quality of Southern Ocean circulation in CMIP5 AOGCM and Earth system model simulations. *Journal of Climate*, *32*, 5915–5940. https://doi.org/10.1175/jcli-d-19-0263.1

Beadling, R. L., Russell, J. L., Stouffer, R. J., Mazloff, M., Talley, L. D., Goodman, P. J., et al. (2020). Representation of Southern Ocean properties across coupled model intercomparison project generations: CMIP3 to CMIP6. *Journal of Climate*, *33*, 6555–6581. https://doi.org/10.1175/jcli-d-19-0970.1

Bindoff, N. L., Rosenberg, M. A., & Warner, M. J. (2000). On the circulation and water masses over the Antarctic continental slope and rise between 80 and 150°E. *Deep-Sea Research, Part II*, *47*(12), 2299–2326. https://doi.org/10.1016/s0967-0645(00)00038-2

Bintanja, R., van Oldenborgh, G. J., Drijfhout, S. S., Wouters, B., & Katsman, C. A. (2013). Important role for ocean warming and increased ice-shelf melt in Antarctic sea-ice expansion. *Nature Geoscience*, *6*, 376–379. https://doi.org/10.1038/ngeo1767

Bronselaer, B., Russell, J. L., Winton, M., Williams, N. L., Key, R. M., Dunne, J. P., et al. (2020). Importance of wind and meltwater for observed chemical and physical changes in the Southern Ocean. *Nature Geoscience*, *13*, 35–42. https://doi.org/10.1038/s41561-019-0502-8

Bronselaer, B., Winton, M., Griffies, S. M., Hurlin, W. J., Rodgers, K. B., Sergienko, O. V., et al. (2018). Change in future climate due to Antarctic meltwater. *Nature*, *564*, 53–58.

Campbell, E. C., Wilson, E. A., Kent Moore, G. W., Riser, S. C., Brayton, C. E., Mazloff, M. R., & Talley, L. D. (2019). Antarctic offshore polynyas linked to Southern Hemisphere climate anomalies. *Nature*, *570*, 319–325. https://doi.org/10.1038/s41586-019-1294-0

Cheon, W. G., & Gordon, A. L. (2019). Open-ocean polynyas and deep convection in the Southern Ocean. *Scientific Reports*, *9*, 6935. https://doi.org/10.1038/s41598-019-43466-2

Costa, D. P., Klinck, J. M., Hofmann, E. E., Dinniman, M. S., & Burns, J. M. (2008). Upper-ocean variability in west Antarctic Peninsula continental shelf waters as measured using instrumented deals. *Deep-Sea Research, Part II*, *55*, 323–337.

De Conto, R. M., & Pollard, D. (2016). Contribution of Antarctica to past and future sea-level rise. *Nature*, *531*, 591–597. https://doi.org/10.1038/nature17145

Depoorter, M. A., Bamber, J. L., Griggs, J. A., Lenaerts, J. T. M., Ligtenberg, S. R. M., van den Broke, M. R., & Moholdt, G. (2013). Calving fluxes and basal melt rates of Antarctic ice shelves. *Nature*, *502*, 89–92. https://doi.org/10.1038/nature12567

Dinniman, M. S., Asay-Davis, X. S., Galton-Fenzi, B. K., Holland, P. R., Jenkins, A., & Timmermann, R. (2016). Modeling ice shelf/ocean interaction in Antarctic: A review. *Oceanography*, *29*, 144–153. https://doi.org/10.5670/oceanog.2016.106

Doddridge, E. W., Marshall, J., Song, H., Campin, J., & Kelley, M. (2021). Southern ocean heat storage, reemergence, and winter sea ice decline induced by summertime winds. *Journal of Climate*, *34*, 1403–1415. https://doi.org/10.1175/jcli-d-20-0322.1

Dufour, C. O., Morrison, A. K., Griffies, S. M., Frenger, I., Zanowski, H. M., & Winton, M. (2017). Preconditioning of the Weddell Sea polynya by the ocean mesoscale and dense water overflows. *Journal of Climate*, *30*, 7719–7737. https://doi.org/10.1175/jcli-d-16-0586.1

Dunne, J. P., Bociu, I., Bronselaer, B., Guo, H., John, J. G., Krasting, J. P., et al. (2020). Simple global ocean Biogeochemistry with Light, Iron, Nutrients and Gas version 2 (BLINGv2): Model description and simulation characteristics in GFDL's CM4.0. *Journal of Advances in Modeling Earth Systems*, *12*, e2019MS002008. https://doi.org/10.1029/2019ms002008

Dunne, J. P., Horowitz, L. W., Adcroft, A. J., Ginoux, P., Held, I. M., John, J. G., et al. (2020). The GFDL Earth system model version 4.1 (GFDL-ESM4.1): Overall coupled model description and simulation characteristics. *Journal of Advances in Modeling Earth Systems*, *12*, e2019MS002015. https://doi.org/10.1029/2019ms002015

Eyring, V., Bony, S., Meehl, G. A., Senior, C. A., Stevens, B., Stouffer, R. J., & Taylor, K. E., (2016). Overview of the coupled model intercomparison project phase 6 (CMIP6) experimental design and organization. *Geoscientific Model Development*, *9*, 1937–1958. https://doi.org/10.5194/gmd-9-1937-2016

Fogwill, C. J., Phipps, S. J., Turney, C. S. M., & Golledge, N. R. (2015). Sensitivity of the Southern Ocean to enhanced regional Antarctic Ice Sheet meltwater input. *Earth's Future*, *3*, 317–329. https://doi.org/10.1002/2015ef000306

Fox-Kemper, B., Danabasoglu, G., Ferrari, R., Griffies, S. M., Hallberg, R. W., Holland, M. M., et al. (2011). Parameterization of mixed layer eddies. III: Implementation and impact in global ocean climate simulations. *Ocean Modelling*, *39*, 61–78. https://doi.org/10.1016/j.ocemod.2010.09.002

Frölicher, T. L., Sarmiento, J. L., Paynter, D. J., Dunne, J. P., Krasting, J. P., & Winton, M. (2015). Dominance of the Southern Ocean in anthropogenic carbon and heat uptake in CMIP5 models. *Journal of Climate*, *28*, 862–886. https://doi.org/10.1175/jcli-d-14-00117.1

Goddard, P. B., Dufour, C. O., Yin, J., Griffies, S. M., & Winton, M. (2017). CO_2-induced ocean warming of the Antarctic continental shelf in an eddying global climate model. *Journal of Geophysical Research: Oceans*, *122*, 8079–8101. https://doi.org/10.1002/2017jc012849

Golledge, N. R., Keller, E. D., Gomez, N., Naughten, K. A., Bernales, J., Trusel, L. D., & Edwards, T. L. (2019). Global environmental consequences of twenty-first-century ice-sheet melt. *Nature*, *566*, 65–72. https://doi.org/10.1038/s41586-019-0889-9

Gordon, A. L. (1978). Deep Antarctic convection west of Maud rise. *Journal of Physical Oceanography*, *8*, 600–612. https://doi.org/10.1175/1520-0485(1978)008<0600:dacwom>2.0.co;2

Goyal, R., Gupta, A. S., Jucker, M., & England, M. H. (2021). Historical and projected changes in the Southern Hemisphere surface westerlies. *Geophysical Research Letters*, *48*, e2020GL090849. https://doi.org/10.1029/2020gl090849

21699291, 2022, 5, Downloaded from https://agupubs.onlinelibrary.wiley.com/doi/10.1029/2021JC017608 by University Of St Andrews University, Wiley Online Library on [08/11/2022]. See the Terms and Conditions (https://onlinelibrary.wiley.com/terms-and-conditions) on Wiley Online Library for rules of use; OA articles are governed by the applicable Creative Commons License

Gregory, J. M., Bouttes, N., Griffies, S. M., Haak, H., Hurlin, W. J., Jungclaus, J., et al. (2016). The flux-anomaly-forced model intercomparison project (FAFMIP) contribution to CMIP6: Investigation of sea-level and ocean climate change in response to CO2 forcing. *Geoscientific Model Development*, *9*, 3993–4017. https://doi.org/10.5194/gmd-9-3993-2016

Griffies, S. M., Adcroft, A. J., & Hallberg, R. W. (2020). A primer on the vertical Lagrangian-remap method in ocean models based on finite-volume generalized vertical coordinates. *Journal of Advances in Modeling Earth Systems*, *12*, e2019MS001954. https://doi.org/10.1029/2019ms001954

Hallberg, R. (2013). Using a resolution function to regulate parameterizations of oceanic mesoscale eddy effects. *Ocean Modelling*, *72*, 92–103. https://doi.org/10.1016/j.ocemod.2013.08.007

Hallberg, R., & Gnanadesikan, A. (2006). The role of eddies in determining the structure and response of the wind-driven Southern Hemisphere overturning: Results from the modeling eddies in the Southern Ocean (MESO) project. *Journal of Physical Oceanography*, *36*, 2232–2252. https://doi.org/10.1175/jpo2980.1

Held, I. M., Guo, H., Adcroft, A., Dunne, J. P., Horowitz, L. W., Krasting, J., et al. (2019). Structure and performance of GFDL's CM4.0 climate model. *Journal of Advances in Modeling Earth Systems*, *11*, 3691–3727.

Heuze, C. (2021). Antarctic bottom water and North Atlantic deep water in CMIP6 models. *Ocean Science*, *17*, 59–90. https://doi.org/10.5194/os-17-59-2021

Heywood, K. J., Muench, R., & Williams, G. (2012). An overview of the Synoptic Antarctic Shelf– Slope Interactions (SASSI) project for the international polar year. *Ocean Science*, *8*, 1111–1116. https://doi.org/10.5194/os-8-1111-2012

Heywood, K. J., Schmidtko, S., Heuzé, C., Kaiser, J., Jickells, T. D., Queste, B. Y., et al. (2014). Ocean processes at the Antarctic continental slope. *Philosophical Transactions of the Royal Society A*, *372*, 20130047. https://doi.org/10.1098/rsta.2013.0047

Horowitz, L. W., Naik, V., Paulot, F., Ginoux, P. A., Dunne, J. P., Mao, J., et al. (2020). The GFDL global atmospheric chemistry-climate model AM4.1: Model description and simulation characteristics. *Journal of Advances in Modeling Earth Systems*, *12*, e2019MS002032. https://doi.org/10.1029/2019ms002032

Huneke, W. G. C., Morrison, A. K., & Hogg, A. M. C. (2022). Spatial and subannual variability of the Antarctic Slope Current in an eddying ocean-sea ice model. *Journal of Physical Oceanography*, *52*. https://doi.org/10.1175/jpo-d-21-0143.1

Jacobs, S. S. (1991). On the nature and significance of the Antarctic Slope Front. *Marine Chemistry*, *35*, 9–24. https://doi.org/10.1016/s0304-4203(09)90005-6

Lago, V., & England, M. H. (2019). Projected slowdown of Antarctic Bottom Water formation in response to amplified meltwater contributions. *Journal of Climate*, *32*, 6319–6335. https://doi.org/10.1175/jcli-d-18-0622.1

Lockwood, J. W., Dufour, C. O., Griffies, S. M., & Winton, M. (2021). On the role of the Antarctic Slope Front on the occurrence of the Weddell Sea polynya under climate change. *Journal of Climate*, *34*, 2529–2548. https://doi.org/10.1175/jcli-d-20-0069.1

Ma, H., & Wu, L. (2011). Global teleconnections in response to freshening over the Antarctic Ocean. *Journal of Climate*, *24*, 1071–1088. https://doi.org/10.1175/2010jcli3634.1

Mackie, S., Smith, I. J., Ridley, J. K., Stevens, D. P., & Langhorne, P. J. (2020). Climate response to increasing Antarctic iceberg and ice shelf melt. *Journal of Climate*, *33*, 8917–8938.

Mathiot, P., Goosse, H., Fichefet, T., Barnier, B., & Gallee, H. (2011). Modeling the seasonal variability of the Antarctic slope current. *Ocean Science*, *7*, 455–470. https://doi.org/10.5194/os-7-455-2011

Mazloff, M., Heimbach, P., & Wunsch, C. (2010). An eddy-permitting Southern Ocean state estimate. *Journal of Physical Oceanography*, *40*, 880–899. https://doi.org/10.1175/2009jpo4236.1

Meijers, A. J. S. (2014). The Southern Ocean in the coupled model intercomparison project phase 5. *Philosophical Transactions of the Royal Society A*, *372*, 20130296. https://doi.org/10.1098/rsta.2013.0296

Meijers, A. J. S., Klocker, A., Bindoff, N. L., Williams, G. D., & Marsland, S. J. (2010). The circulation and water masses of the Antarctic shelf and continental slope between 30 and 80°E. *Deep Sea Research Part II: Topical Studies in Oceanography*, *57*, 723–737. https://doi.org/10.1016/j.dsr2.2009.04.019

Meinshausen, M., Nicholls, Z. R. J., Lewis, J., Gidden, M. J., Vogel, E., Freund, M., et al. (2020). The shared socio-economic pathway (SSP) greenhouse gas concentrations and their extension to 2500. *Geoscientific Model Development*, *13*, 3571–3605. https://doi.org/10.5194/gmd-13-3571-2020

Menviel, L., Timmermann, A., Timm, O. E., & Mouchet, A. (2010). Climate and biogeochemical response to a rapid melting of the West Antarctic Ice Sheet during interglacials and implications for future climate. *Paleoceanography*, *25*, PA4231. https://doi.org/10.1029/2009pa001892

Moorman, R., Morrison, A. K., & Hogg, A. M. C. (2020). Thermal responses to Antarctic ice shelf melt in an eddy-rich global ocean-sea ice model. *Journal of Climate*, *33*, 6599–6620. https://doi.org/10.1175/jcli-d-19-0846.1

Morrison, A. K., & Hogg, A. M. C. (2013). On the relationship between Southern Ocean overturning and ACC transport. *Journal of Physical Oceanography*, *43*, 140–148. https://doi.org/10.1175/jpo-d-12-057.1

Morrison, A. K., Hogg, A. M. C., England, M. H., & Spence, P. (2020). Warm Circumpolar Deep Water transport toward Antarctica driven by local dense water export in canyons. *Science Advances*, *6*, eaav2516. https://doi.org/10.1126/sciadv.aav2516

Oppenheimer, M., Glavovic, B. C., Hinkel, J., van de Wal, R., Magnan, A. K., Abd-Elgawad, A., et al. (2019). Sea level rise and implications for low-lying islands, coasts and communities. In D. C. Roberts, V. Masson-Delmotte, P. Zhai, M. Tignor, E. Poloczanska, K. Mintenbeck, A. Alegría, M. Nicolai, A. Okem, J. Petzold, B. Rama, & N. M. Weyer (Eds.), *IPCC special report on the ocean and cryosphere in a changing climate [H.-O. Pörtner]*. In press.

Paolo, F. S., Fricker, H. A., & Padman, L. (2015). Volume loss from Antarctic ice shelves is accelerating. *Science*, *348*, 327–331. https://doi.org/10.1126/science.aaa0940

Pauling, A. G., Bitz, C. M., Smith, I. J., & Langhorne, P. J. (2016). The response of the Southern Ocean and Antarctic sea ice to freshwater from ice shelves in an Earth system model. *Journal of Climate*, *29*, 1655–1672. https://doi.org/10.1175/jcli-d-15-0501.1

Pedlosky, J. (1987). *Geophysical fluid dynamics*. Springer Verlag New York.

Peña-Molino, B., McCartney, M. S., & Rintoul, S. R. (2016). Direct observations of the Antarctic slope current transport at 113°E. *Journal of Geophysical Research: Oceans*, *121*, 7390–7407. https://doi.org/10.1002/2015jc011594

Purich, A., & England, M. H. (2021). Historical and future projected warming of Antarctic Shelf Bottom Water in CMIP6 models. *Geophysical Research Letters*, *48*. https://doi.org/10.1029/2021gl092752

Purich, A., England, M. H., Cai, W., Sullivan, A., & Durack, P. J. (2018). Impacts of broad-scale surface freshening of the Southern Ocean in a coupled climate model. *Journal of Climate*, *31*, 2613–2632. https://doi.org/10.1175/jcli-d-17-0092.1

Riahi, K., Rao, S., Krey, V., Cho, C., Chrikov, V., Fischer, G., et al. (2011). RCP 8.5—A scenario of comparatively high greenhouse gas emissions. *Climate Change*, *109*, 33. https://doi.org/10.1007/s10584-011-0149-y

21699291, 2022, 5, Downloaded from https://agupubs.onlinelibrary.wiley.com/doi/10.1029/2021JC017608 by University Of St Andrews University, Wiley Online Library on [08/11/2022]. See the Terms and Conditions (https://onlinelibrary.wiley.com/terms-and-conditions) on Wiley Online Library for rules of use; OA articles are governed by the applicable Creative Commons License

Riechl, B. G., & Hallberg, R. (2018). A simplified energetics based planetary boundary layer (ePBL) approach for ocean climate simulations. *Ocean Modelling*, *132*, 112–129.

Rignot, E., Jacobs, S., Mouginot, J., & Scheuchl, B. (2013). Ice-shelf melting around Antarctica. *Science*, *341*, 266–270. https://doi.org/10.1126/science.1235798

Rignot, E., Mouginot, J., Scheuchl, B., van den Broeke, M., van Wessem, M. J., & Morlighem, M. (2019). Four decades of Antarctic Ice Sheet mass balance from 1979–2017. *Proceedings of the National Academy of Sciences of the United States of America*, *116*, 1095–1103. https://doi.org/10.1073/pnas.1812883116

Roemmich, D., Church, J., Gilson, J., Monselesan, D., Sutton, P., & Wijffels, S. (2015). Unabated planetary warming and its ocean structure since 2006. *Nature Climate Change*, *5*, 240–245.

Russell, J. L., Dixon, K. W., Gnanadesikan, A., Stouffer, R. J., & Toggweiler, J. R. (2006). The Southern Hemisphere westerlies in a warming world: Propping open the door to the deep ocean. *Journal of Climate*, *19*, 6382–6390. https://doi.org/10.1175/jcli3984.1

Sadai, S., Condron, A., DeConto, R., & Pollard, D. (2020). Future climate response to Antarctic Ice Sheet melt caused by anthropogenic warming. *Science Advances*, *6*, eaaz1169. https://doi.org/10.1126/sciadv.aaz1169

Sallée, J. B., Shuckburgh, E., Bruneau, N., Meijers, A. J. S., Bracegirdle, T. J., Wang, Z., & Roy, T., (2013). Assessment of Southern Ocean water mass circulation and characteristics in CMIP5 models: Historical bias and forcing response. *Journal of Geophysical Research: Oceans*, *118*, 1830–1844. https://doi.org/10.1002/jgrc.20135

Schloesser, F., Friedrich, T., Timmermann, A., DeConto, R. M., & Pollard, D. (2019). Antarctic iceberg impacts on future Southern Hemisphere climate. *Nature Climate Change*, *9*, 672–677. https://doi.org/10.1038/s41558-019-0546-1

Shepherd, A., Wingham, D., & Rignot, E. (2004). Warm ocean is eroding West Antarctic Ice Sheet. *Geophysical Research Letters*, *31*, L23402. https://doi.org/10.1029/2004gl021106

Snow, K., Hogg, A. M., Sloyan, B. M., & Downes, S. M. (2016). Sensitivity of Antarctic Bottom Water to changes in surface buoyancy fluxes. *Journal of Climate*, *29*, 313–330. https://doi.org/10.1175/jcli-d-15-0467.1

Spence, P., Griffies, S. M., England, M. H., Hogg, A. M., Saenko, O. A., & Jourdain, N. C. (2014). Rapid subsurface warming and circulation changes of Antarctic coastal waters by poleward shifting winds. *Geophysical Research Letters*, *41*, 4601–4610. https://doi.org/10.1002/2014gl060613

Spence, P., Holmes, R. M., Hogg, A. M., Griffies, S. M., Stewart, K. D., & England, M. H., (2017). Localized rapid warming of West Antarctic subsurface waters by remote winds. *Nature Climate Change*, *7*, 595–603.

Stern, A. A., Adcroft, A., & Sergienko, O. (2016). The effects of Antarctic iceberg calving-size distribution in a global climate model. *Journal of Geophysical Research: Oceans*, *121*, 5773–5788. https://doi.org/10.1002/2016jc011835

Stewart, A. L., Klocker, A., & Menemenlis, D. (2019). Acceleration and overturning of the Antarctic Slope Current by winds, eddies, and tides. *Journal of Physical Oceanography*, *49*, 2043–2074. https://doi.org/10.1175/jpo-d-18-0221.1

Stewart, A. L., & Thompson, A. F. (2015). Eddy-mediated transport of warm circumpolar deep water across the Antarctic shelf break. *Geophysical Research Letters*, *42*, 432–440. https://doi.org/10.1002/2014gl062281

Stewart, K. D., & Haine, T. W. N. (2016). Thermobaricity in the Transition Zones between alpha and beta oceans. *Journal of Physical Oceanography*, *46*, 1805–1821. https://doi.org/10.1175/jpo-d-16-0017.1

Stock, C. A., Dunne, J. P., Fan, S., Ginoux, P., John, J., Krasting, J. P., et al. (2020). Ocean biogeochemistry in GFDL's Earth System Model 4.1 and its response to increasing atmospheric CO2. *Journal of Advances in Modeling Earth Systems*, *12*, e2019MS002043. https://doi.org/10.1029/2019ms002043

Stouffer, R. J., Seidov, D., & Haupt, B. J. (2007). Climate response to external sources of freshwater: North Atlantic versus the Southern Ocean. *Journal of Climate*, *20*, 436–448. https://doi.org/10.1175/jcli4015.1

Swart, N. C., & Fyfe, J. C. (2012). Observed and simulated changes in the Southern Hemisphere surface westerly wind-stress. *Geophysical Research Letters*, *39*, L16711. https://doi.org/10.1029/2012gl052810

Swart, N. C., & Fyfe, J. C. (2013). The influence of recent Antarctic Ice Sheet retreat on simulated sea ice area trends. *Geophysical Research Letters*, *40*, 4328–4332. https://doi.org/10.1002/grl.50820

Swingedouw, D., Fichefet, T., Goosse, H., & Loutre, M. F. (2009). Impact of transient freshwater releases in the Southern Ocean on the AMOC and climate. *Climate Dynamics*, *33*, 365–381. https://doi.org/10.1007/s00382-008-0496-1

The IMBIE team. (2018). Mass balance of the Antarctic Ice Sheet from 1992 to 2017. *Nature*, *558*, 219–222.

Thompson, A. F., Stewart, A. L., Spence, P., & Heywood, K. J. (2018). The Antarctic Slope Current in a changing climate. *Reviews of Geophysics*, *56*, 741–770. https://doi.org/10.1029/2018rg000624

Thompson, D. W. J., Solomon, S., Kushner, P. J., England, M. H., Grise, K. M., & Karoly, D. J. (2011). Signatures of the Antarctic ozone hole in Southern Hemisphere surface climate change. *Nature Geoscience*, *4*, 741–749. https://doi.org/10.1038/ngeo1296

Waugh, D. W., Hogg, A. M. C., Spence, P., England, M. H., & Haine, T. W. N. (2019). Response of Southern Ocean ventilation to changes in midlatitude westerly winds. *Journal of Climate*, *32*, 5345–5361. https://doi.org/10.1175/jcli-d-19-0039.1

Waugh, D. W., Stewart, K., Hogg, A. M., & England, M. H. (2021). Interbasin differences in ocean ventilation in response to variations in the Southern Annular Mode. *Journal of Geophysical Research: Oceans*, *126*, e2020JC016540. https://doi.org/10.1029/2020jc016540

Whitworth, T., Orsi, A. H., Kim, S.-J., Nowlin, W. D., & Locarnini, R. A. (1998). Water masses and mixing near the Antarctic slope front. Ocean, ice, and atmosphere: Interactions at the Antarctic continental margin. In S. S. Jacobs, & R. F. Weiss (Eds.), *Antarctic Research Series* (Vol. 75, pp. 1–27). American Geophysical Union.

Xu, X., Chassignet, E. P., Firing, Y. L., & Donohue, K. (2020). Antarctic Circumpolar Current transport through Drake Passage: What can we learn from comparing high-resolution model results to observations? *Journal of Geophysical Research: Oceans*, *125*, e2020JC016365. https://doi.org/10.1029/2020jc016365

Zhao, M., Golaz, J.-C., Held, I. M., Guo, H., Balaji, V., Benson, R., et al. (2018a). The GFDL global atmosphere and land model AM4. 0/LM4. 0: 1. Simulation characteristics with prescribed SSTs. *Journal of Advances in Modeling Earth Systems*, *10*, 735–769.

Zhao, M., Golaz, J.-C., Held, I. M., Guo, H., Balaji, V., Benson, R., et al. (2018b). The GFDL global atmosphere and land model AM4. 0/LM4.1360 0: 2. Model description, sensitivity studies, and tuning strategies. *Journal of Advances in Modeling Earth Systems*, *10*, 691–734.

21699291, 2022, 5, Downloaded from https://agupubs.onlinelibrary.wiley.com/doi/10.1029/2021JC017608 by University Of St Andrews University, Wiley Online Library on [08/11/2022]. See the Terms and Conditions (https://onlinelibrary.wiley.com/terms-and-conditions) on Wiley Online Library for rules of use; OA articles are governed by the applicable Creative Commons License